GANIL

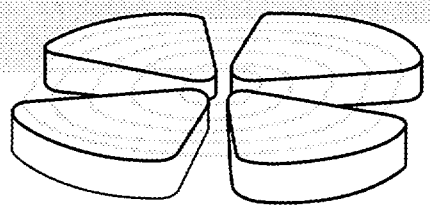

Study of the $^7Be(p,\gamma)^8B$ and $^7Li(n,\gamma)^8Li$ capture reactions using the shell model embedded in the continuum

K. Bennaceur†, F. Nowacki†‡, J. Okołowicz†§ and M. Płoszajczak†

† *Grand Accélérateur National d'Ions Lourds (GANIL), CEA/DSM - CNRS/IN2P3, BP 5027, F-14076 Caen Cedex 05, France*

‡ *Laboratoire de Physique Théorique Strasbourg (EP 106), 3-5 rue de l'Universite, F-67084 Strasbourg Cedex, France*

§ *Institute of Nuclear Physics, Radzikowskiego 152, PL - 31342 Krakow, Poland*

GANIL P 99 02

Study of the $^7Be(p,\gamma)^8B$ and $^7Li(n,\gamma)^8Li$ capture reactions using the shell model embedded in the continuum

K. Bennaceur†, F. Nowacki†‡, J. Okołowicz†§ and M. Płoszajczak†

† *Grand Accélérateur National d'Ions Lourds (GANIL), CEA/DSM - CNRS/IN2P3, BP 5027, F-14076 Caen Cedex 05, France*

‡ *Laboratoire de Physique Théorique Strasbourg (EP 106), 3-5 rue de l'Universite, F-67084 Strasbourg Cedex, France*

§ *Institute of Nuclear Physics, Radzikowskiego 152, PL - 31342 Krakow, Poland*

(February 2, 1999)

Abstract

We apply the realistic shell model which includes the coupling between many-particle (quasi-)bound states and the continuum of one-particle scattering states to the spectroscopy of mirror nuclei: ^{8}B and ^{8}Li, as well as to the description of low energy cross sections (the astrophysical S factors) in the capture reactions: ^{7}Be$(p,\gamma)^8$B and ^{7}Li$(n,\gamma)^8$Li .

21.60.Cs, 24.10.Eq, 25.40.Lw, 27.20.+n

I. INTRODUCTION

The solution of solar neutrino problem, *i.e.*, an observed deficit of neutrinos with respect to predictions of the Standard Solar Model (SSM) [1] , is passing through an understanding of the capture reaction: $^7\mathrm{Be}(p,\gamma)^8\mathrm{B}$. The ^{8}B produced in the solar interior in the reaction $^7\mathrm{Be}(p,\gamma)^8\mathrm{B}$, is the principal source of high energy neutrinos detected in solar neutrino experiments. Therefore, if we stay within the framework of standard electroweak theory and the SSM [2], the observed deficit of those neutrinos can be traced back, at least partially, to the value of low energy $^7\mathrm{Be}(p,\gamma)^8\mathrm{B}$ radiative capture cross section which determines the magnitude of neutrino flux and remains the most uncertain quantity in the SSM [2]. At the solar energies ($\sim 20\,\mathrm{keV}$), this cross-section is too small to be directly measurable. For this reason, the theoretical analysis of this reaction is so important. On the other hand, whenever the measurement is feasible ($E_{CM} > 150\,\mathrm{keV}$), the exact value of the capture cross section depends : (i) on the normalization obtained indirectly from the $^7\mathrm{Li}(d,p)^8\mathrm{Li}$ cross section and, (ii) on the model dependent extrapolation of measured values of the cross-section down to the interesting domain of solar energies. Experimental data for the $^7\mathrm{Be}(p,\gamma)^8\mathrm{B}$ capture cross section are varying strongly [3–7] , though more recent experiments consistently indicate low values ($S < 20$ eV·b) for the astrophysical factor $S \equiv \sigma_{CM}(E_{CM})E_{CM}\exp(-2\pi\eta)$, where $\eta = e^2 Z_1 Z_2/\hbar v$ [6,7]. Also the Coulomb dissociation experiments [8] deduce low value for the astrophysical S - factor though this value depends strongly on the amount of $E2$ - contribution in the Coulomb dissociation which is not yet completely understood.

Many different theoretical models have been applied for the calculation of S - factor at stellar energies [9–16], and their predictions are often in striking disagreement among each other, confirming strong model and/or approximation dependence of calculated cross-section. Part of the theoretical ambiguities can be removed by a simultaneous study of the $^7\mathrm{Li}(n,\gamma)^8\mathrm{Li}$ mirror reaction, which has also been studied by several experimental groups [17–19]. Also for this reaction, largely different values for the low energy capture cross section have been reported [17–19]. In the context of the solar neutrino

problem, the ^{7}Li$(n,\gamma)^8$Li cross section is often used to extrapolate the capture cross section for the reaction ^{7}Be$(p,\gamma)^8$B down to the solar energies at $E_{CM} \sim 20\,$keV [6] . But the ^{7}Li$(n,\gamma)^8$Li reaction cross section at very low energies is also extremely interesting in itself as it provides the essential element of rapid process of primordial nucleosynthesis of nuclei with $A \geq 12$ in the inhomogeneous big-bang models [20–23]. Indeed, in the inhomogeneous big-bang hypothesis [20–23], the main reaction chain leading to the synthesis of heavy elements is [22] ^{1}H$(n,\gamma)^2$H$(n,\gamma)^3$H$(d,n)^4$He$(t,\gamma)^7$Li$(n,\gamma)^8$Li, and then ^{8}Li$(\alpha,n)^{11}$B$(n,\gamma)^{12}$B$(\beta^-)^{12}C(n,\gamma)^{13}$C, *etc.*, for heavier nuclei. In this sense, the reaction ^{7}Li$(n,\gamma)^8$Li is a key process to bridge the gap of mass $A = 8$ and to produce heavy elements.

The theoretical description of weakly bound exotic nuclei close to the drip-line, such as, *e.g.*, ^{8}B on the proton rich side of the drip line or ^{11}Be, ^{11}Li on the neutron rich side of the drip line, is challenging due to the proximity of particle continuum which implies the strong modification of effective nucleon - nucleon interaction and causes the unusual spatial properties (halo structures, a large diffusivity) of nucleon density distribution . Nowadays, these properties are perhaps somewhat better understood near the neutron drip line than near the proton drip line. In weakly bound exotic nuclei, number of excited bound states or narrow resonances is small and , moreover, they couple strongly to the particle continuum. Hence, these systems should be described in the quantum open system formalism which does not artificially separate the subspaces of (quasi-) bound (the Q-subspace) and scattering (the P-subspace) states. For well bound nuclei close to the β - stability line, microscopic description of states in the first subspace is given by the nuclear shell model (SM) with model-space dependent effective two-body interactions, whereas the latter subspace is treated in terms of the coupled channels equations. For weakly bound exotic nuclei, the validity of this basic paradigm is certainly questionable, and we propose to change it by considering the approximation which takes into account coupling between Q and P subspaces in terms of the residual nucleon–nucleon interaction. This coupling will consistently modify both the scattering solutions and the spectroscopic quantities for interior bound states.

One possibility for such an approach could be the Continuum Shell Model (CSM) , which in the restricted space of configurations generated using the finite-depth potential has been studied for the giant resonances and for the radiative capture reactions probing the microscopic structure of these resonances [24–27] . This approach may be insufficient for the description of low lying excitations, in particular in the nuclei close to drip lines, where it is essential to have a most realistic description of bound states. For that reason, the cornerstone of our approach, which is called in the following the Shell Model Embedded in the Continuum (SMEC), is the *realistic* SM itself which is used to generate the N-particle wave functions. This choice implies that coupling between the SM states and the one-particle scattering continuum must be given by the residual nucleon - nucleon interaction. The first application of the SMEC model has been published recently in Ref. [29] .

As said before, we are interested in describing low lying bound and resonance states in exotic nuclei. For that reason, we restrict the description of particle continuum to the subset of one-nucleon decay channels. This should be a reasonable starting point for describing both the microscopic structure of ^{8}B and ^{8}Li and the corresponding reactions: ^{7}Be$(p,\gamma)^8$B and ^{7}Li$(n,\gamma)^8$Li. Also at higher energies above, *e.g.*, α or t emission thresholds, the one-particle continuum approximation prohibits a reliable description of more complicated multi-nucleon decay channels as well as the residual correlations generated in the many-body wave functions of bound states by the coupling to those channels. In principle, this obstacle can be removed in future studies and further improvement of the SMEC (CSM) to include more complicated channels like, *e.g.*, the α - decay channel, can be done following the approach of Balashov et al. [30] . This rather involved extension of the SMEC (CSM) will not be discussed here any further. One should also be aware that in the case of two-nucleon halo nuclei or at higher energies above the threshold for the three-particle decay, the one-particle continuum approximation is oversimplified.

The paper is constructed in the following way. In Sect. 2, we present some details of the SMEC model, stressing in particular those elements which differ this model from the CSM. Sect. 3 is devoted to the discussion of spectroscopic properties of ^{8}B (Sect. 3.1) and

^{8}Li (Sect. 3.2). We shall discuss influence of the residual interaction which couples Q and P subspaces on the energy and the width of many-body states. We will also discuss an important self-consistency correction to the average single particle (s.p.) potential which results from this residual interaction. The self-consistent average potential is then used to generate radial formfactors of many-body states which enter the coupling matrix elements between Q and P subspaces. Sect. 4 is devoted to the discussion of ^{7}Be$(p,\gamma)^8$B and and ^{7}Li$(n,\gamma)^8$Li capture cross sections. Finally, the most important conclusions are summarized in Sect. 5.

II. THE SHELL MODEL EMBEDDED IN THE CONTINUUM (SMEC)

In the decaying nucleus or in the reaction processes such as, *e.g.*, the radiative capture process, all asymptotic channels are given by the solutions with outgoing waves. Such physical systems, in which bound (localized) interior states are coupled to the asymptotic scattering channels, are called the open systems. One way out of this complication is to describe the quantum open system *together* with its environment of asymptotic channels as the quantum closed system. This implies that the projection operator technique is used to separate P subspace of asymptotic channels from the Q subspace of many-body states which are build up by the bound s.p. wave functions and by the s.p. resonance wave functions. In this latter case, one should use certain cutoff radius to define this part of resonance wave function which belongs to the Q subspace and the remaining part is put into the P subspace. In our case, the P subspace contains $(N-1)$ - particle states with nucleons on bound orbits and one nucleon in the scattering state, but also this part of the s.p. resonance wave functions which is outside of the cutoff radius. In fact, we define the P subspace from the condition

$$P + Q = 1 \quad , \tag{1}$$

which also implies that all wave functions used in the calculations are orthonormalized in the usual sense. Physically, the closeness assumption for the total system means that the

states of $(N-1)$ - nucleus which define the asymptotic channels for the studied reaction are assumed to be stable. This assumption in turn means that the most important channels are supposed to be those which involve low-lying states of the residual nucleus. In the domain of low energy excitations and/or for weakly bound nuclei away from the β-stability line this is most likely a good approximation. However, in the domain of higher excitation like, *e.g.*, for the giant resonances, the quality of this approximation which depends on the width of considered many-body states in $N-1$ nucleus, may be hazardous for broad states.

The key element of the CSM is the treatment of s.p. resonances, which on one side may have an important amplitude inside a nucleus and, on other side, they exhibit asymptotic behaviour of scattering wave functions [24] . The part of resonance for $r < R_{cut}$, where R_{cut} is the cut-off radius, is included in Q subspace, whereas the remaining part is left in the P subspace [24]. The wave functions of both subspaces are then renormalized in order to ensure the orthogonality of wave functions in both subspaces. It should be mentioned that in the earlier formulation of the CSM [28], the contribution of the s.p. resonances both to Q and P subspaces have been neglected.

In the SMEC calculations, we solve similar equations as in the CSM [24] but , as explained below, due to specificity of exotic nuclei, we change certain important ingredients of the CSM. For the bound states we solve the standard SM problem:

$$H_{QQ}\Phi_i = E_i\Phi_i \quad . \tag{2}$$

$H_{QQ} \equiv QHQ$ is *identified* with the SM Hamiltonian and its Φ_i are the N-particle (quasi-) bound wave functions. We believe, that for a quantitative description of low lying states in the exotic nuclei one has to use as a starting point the accurate many-body wave functions in the Q subspace which are provided by the SM with effective interactions.

The residual coupling of P and Q subspaces is given by the zero-range force

$$V_{12} = -V_{12}^{(0)}[\alpha + (1-\alpha)P_{12}^{\sigma}]\delta(\mathbf{r}_1 - \mathbf{r}_2) \quad , \tag{3}$$

where P_{12}^{σ} is the spin exchange operator. We assume that the SM Hamiltonian H_{QQ} contains already effects generated by this residual coupling and we do not modify H_{QQ} anymore.

For the continuum part, we solve the coupled channel equations:

$$(E^{(+)} - H_{PP})\xi_E^{c(+)} = 0 \quad , \tag{4}$$

where index c denotes different channels and $H_{PP} \equiv PHP$. The superscript $(+)$ in (4) means that boundary conditions for outgoing scattering waves are used. In our case, we have ingoing wave in the input channel and outgoing waves in all other channels. The structure of $(N-1)$ - nucleus is given by the SM, whereas one nucleon occupies a scattering state. The channel states are defined by coupling one nucleon in the continuum to a many-body state of $(N-1)$ - nucleus.

The SM wave function has an incorrect asymptotic radial behaviour for unbound states. Therefore, to generate both the radial s.p. wave functions in the Q space and the scattering wave functions in P space we use the finite-depth average potential of Saxon-Woods (SW) type with the spin-orbit part included:

$$U(r) = V_0 f(r) + V_{SO}(4\mathbf{l}\cdot\mathbf{s})\frac{1}{r}\frac{df(r)}{dr} + V_C \quad , \tag{5}$$

where $f(r)$ is the spherical symmetric SW formfactor:

$$f(r) = \left[1 + \exp\left(\frac{r-R_0}{a}\right)\right]^{-1} \quad . \tag{6}$$

The Coulomb potential V_C is calculated for the uniformly charged sphere with radius R_0.

Coupled channel eqs. (4) can be written more explicitly as:

$$\sum_{c'}(E^{(+)} - H_{cc'})\xi_E^{c'(+)} = 0 \quad , \tag{7}$$

where

$$H_{cc'} = (T+U)\delta_{cc'} + v^J_{cc'} \quad . \tag{8}$$

In the above equation, T stands for the kinetic-energy operator and $v^J_{cc'}$ is the channel-channel coupling generated by the residual interaction. The explicit formula for $v^J_{cc'}$ is given in (A4). The s.p. potential in (8) consists of an 'initial guess' $U(r)$, and the diagonal part of

the coupling potential v_{cc}^{J} which depends on both the s.p. orbit $\phi_{l,j}$ and the considered many-body state J^{π}. Obviously, this correction cannot be neglected when generating s.p. wave function $\phi_{l,j}$ for a given J^{π}. These s.p. wave functions define Q subspace and thus modify the diagonal part of the residual force. So this implies a self-consistent iterative procedure, because the change of s.p. wave function changes in turn the correction coming from the residual force (see the Appendix A). As long as this correction is small in comparison with the initial average potential, the iterative procedure is fastly converging to the new self-consistent average potential:

$$U^{(sc)}(r) = U(r) + v_{cc}^{J(sc)}(r) \quad . \tag{9}$$

The parameters of the initial average potential (5) are chosen in such a way that the resulting potential $U^{(sc)}(r)$ reproduces energies of experimental s.p. states, whenever their identification is possible. In the next section, we will show examples of such self-consistent potentials. The dependence of the generated correction in the potential (9) on isospin of s.p. states generates a mutual dependence of average potentials for protons and neutrons in the iterative procedure. Using self-consistently determined radial wave functions instead of those generated by $U(r)$ means that the matrix elements $V_{\alpha\beta\gamma\delta}$ (A1) of the residual force V_{12} depend not only on the s.p. wave functions $\phi_{l,j}$ involved but also on the many-body state J^{π}. This is another interesting aspect of the self-consistent procedure determining the average potential in SMEC.

The third system of equations in CSM consists of inhomogeneous coupled channel equations:

$$(E^{(+)} - H_{PP})\omega_i^{(+)} = H_{PQ}\Phi_i \equiv w_i \tag{10}$$

with the source term w_i which is primarily given by the SM structure of N - particle wave function for state Φ_i . The explicit form of the source term is given in (A7). These equations define functions $\omega_i^{(+)}$, which describe the decay of quasi-bound state Φ_i in the continuum. The source w_i couples the wave function of N - nucleon localized states with $(N-1)$ -

nucleon localized states plus one nucleon in the continuum. For zero-range residual force (3), formfactor of the source term is given by the s.p. wave functions of the same self-consistently determined average potential $U^{(sc)}(r)$ as used to define the subspaces Q and P.

The full solution of the many-body problem can be expressed by means of three distinct functions: Φ_i , ξ^c_E and ω_i , and reads [24] :

$$\Psi^c_E = \xi^c_E + \sum_{i,j}(\Phi_i + \omega_i)\frac{1}{E - H^{eff}_{QQ}} < \Phi_j \mid H_{QP} \mid \xi^c_E > \ , \tag{11}$$

where

$$H^{eff}_{QQ} = H_{QQ} + H_{QP}G^{(+)}_P H_{PQ} \ , \tag{12}$$

is the effective SM Hamiltonian including the coupling to the continuum, and $G^{(+)}_P$ is the Green function for the motion of s.p. in P subspace. Matrix H^{eff}_{QQ} is non-Hermitian (symmetric and complex matrix) for energies above the particle emission threshold and Hermitian (real) for lower energies. Consequently, the eigenvalues of H^{eff}_{QQ} are real for bound states and complex for decaying states. Matrix H^{eff}_{QQ} can be diagonalized by the orthogonal transformation:

$$\Phi_i \longrightarrow \tilde{\Phi}_j = \sum_i b_{ji}\Phi_i \ , \tag{13}$$

with complex eigenvalues: $\tilde{E}_i - \frac{1}{2}i\tilde{\Gamma}_i$, which depend on the energy E of particle in the continuum. The eigenvalues of H^{eff}_{QQ} at energies $\tilde{E}_i(E) = E$, determine the energies and widths of resonance states. With these changes, one obtains:

$$\Psi^c_E = \xi^c_E + \sum_i \tilde{\Omega}_i \frac{1}{E - \tilde{E}_i + (i/2)\tilde{\Gamma}_i} < \tilde{\Phi}_i \mid H \mid \xi^c_E > \tag{14}$$

for the many-body wave function projected on channel c , where

$$\tilde{\Omega}_i = \tilde{\Phi}_i + \sum_c \int_{\varepsilon_c}^{\infty} dE' \xi^c_{E'} \frac{1}{E^{(+)} - E'} < \xi^c_{E'} \mid H \mid \tilde{\Phi}_i > \ , \tag{15}$$

is the wave function of discrete state modified by the coupling to the continuum states. Hence, this formalism if fully *symmetric* in treating the continuum and bound state part

Ψ_E^c (in Eq. (14)) represents the continuum state modified by the discrete states, and $\tilde{\Omega}_i$ (in Eq. (15)) represents the discrete state modified by the coupling to the continuum. More informations about those features of SMEC which are the same as in the CSM, can be found in the paper by Bartz et al. [24].

III. SPECTROSCOPY OF ^{8}B AND ^{8}LI NUCLEI

A. The self-consistent average potential spanning the Q subspace

The essential element of SMEC approach is the construction of Q - subspace. As explained in the previous section, this is obtained by an iterative procedure which for a given initial average s.p. potential (5) and for a given residual two-body interaction (3) yields the self-consistent s.p. potential depending on the s.p. wave function $\phi_{l,j}$, the total spin J of the N-nucleon system as well as on the one-body matrix elements of $(N-1)$ - nucleon daughter system. The parameters of different initial SW potentials for [p $\otimes$ ^{7}Be] and [n $\otimes$ ^{7}Li] systems, which are used in this work are summarized in Table I. These potentials have been obtained for different parameters $(1-\alpha)$ of the spin-exchange component in the residual interaction (3) and for different s.p. orbits $\phi_{l,j}$ which correspond to energies $\varepsilon_{l,j}$ (see the second column in Table I) in the self-consistently determined potential $U^{(sc)}(r)$. In all cases, the strength of the residual interaction (3) is $V_{12}^{(0)} = 650\,\mathrm{MeV{\cdot}fm^3}$. All these potentials have the same parameters of radius $R_0 = 2.4\,\mathrm{fm}$, surface diffuseness $a = 0.52\,\mathrm{fm}$, and spin-orbit coupling $V_{SO} = -4\,\mathrm{MeV}$. Cohen - Kurath (CK) interaction [31] is used as a SM interaction. In Fig. 1 , we show examples of calculated potentials in ^{8}B for the proton s.p. orbital $1p_{3/2}$ in two different total spin states: $J^\pi = 2^+$ and $J^\pi = 1^+$. The calculations have been performed using the initial potential $U(r)$ for $(1-\alpha) = 0.27$, which is chosen in such a way that the self-consistent potential $U^{(sc)}(r)$ yields $1p_{3/2}$ proton s.p. orbit bound at the experimental binding energy of ground state (g.s.) $J^\pi = 2_1^+$. The same $U(r)$ is then taken both for 2^+ and 1^+ states. The spectroscopic factor of proton $1p_{3/2}$ s.p. state in the g.s., is close to 1 for

CK interaction [31]. This allows to identify position of proton $1p_{3/2}$ s.p. orbit in $J^\pi = 2^+$ state, *i.e.*, we demand that $U^{(sc)}(r)$ provides $1p_{3/2}$ s.p. state at $-137\,\mathrm{keV}$. This choice, as we shall see in Sect. 4.A, is essential for a quantitative description of $^7\mathrm{Be}(p,\gamma)^8\mathrm{B}$ radiative capture cross-section.

The self-consistent average potential $U^{(sc)}(r)$ (the solid line in the l.h.s. plot) exhibits for small r a clear maximum which is absent in the initial potential $U(r)$. One should also notice, that self-consistent potentials $U^{(sc)}(2^+)$ and $U^{(sc)}(1^+)$ are different (compare solid curves on l.h.s. and r.h.s. of Fig. 1) , in spite of the fact that the initial potential $U(r)$ in these states is the same. This clearly shows strong state dependence of calculated average fields and two-body effective interactions. For example, whereas the $1p_{3/2}$ s.p. orbit in the g.s. ($J^\pi = 2^+_1$) is at $-137\,\mathrm{keV}$, the self-consistent procedure yields this orbit at $-2.538\,\mathrm{MeV}$ in the first excited state ($J^\pi = 1^+_1$) .

The dotted lines in Fig. 1 show the equivalent s.p. average potentials $U^{(eq)}(r)$ in $J^\pi = 2^+$ and 1^+ states for proton $1p_{3/2}$ orbit. For the same a, R_0 and V_{SO} parameters as in the initial potential $U(r)$, parameter V_0 in $U^{(eq)}(r)$ is adjusted in order to reproduce the energy of $1p_{3/2}$ s.p. orbit in $U^{(sc)}(r)$. Clearly, $U^{(eq)}(r)$ and $U^{(sc)}(r)$ differ strongly in the potential interior. However, the potential surface of $U^{(eq)}(r)$ and $U^{(sc)}(r)$ for both considered J^π is very similar. This is particularly apparent for $J^\pi = 2^+$. The root mean squared (r.m.s.) radius of the $1p_{3/2}$ orbit is $< r^2 >^{1/2} = 4.228\,\mathrm{fm}$ in $U^{(sc)}(2^+)$ and $< r^2 >^{1/2} = 4.239\,\mathrm{fm}$ in $U^{(eq)}(2^+)$. For $J^\pi = 1^+$, the effective surface diffuseness of $U^{(sc)}(r)$ is even slightly decreasing. Also the radial wave functions of the proton $1p_{3/2}$ orbit in $U^{(sc)}(r)$ and $U^{(eq)}(r)$ are almost identical with only a small shift towards the potential interior of the maximum of radial wave function in $U^{(sc)}(r)$.

We have no clear indication concerning the position of proton $1p_{1/2}$ s.p. orbit. Using the same $U(r)$ as used to determine $U^{(sc)}(r)$ for $1p_{3/2}$ s.p. state, we get the $1p_{1/2}$ proton s.p. orbit in $U^{(sc)}(r)$ at $\varepsilon_{p_{1/2}} = +0.731\,\mathrm{MeV}$ in $J^\pi = 2^+$ states and at $\varepsilon_{p_{1/2}} = +0.311\,\mathrm{MeV}$ in $J^\pi = 1^+$ states . Consequently, the energy splitting of $p_{3/2}$ and $p_{1/2}$ orbitals is state dependent. It is $\Delta\varepsilon = 3.369\,\mathrm{MeV}$, in the initial potential $U(r)$. In $U^{(sc)}(r)$, it equals $\Delta\varepsilon = 0.868\,\mathrm{MeV}$

for $J^\pi = 2^+$, and $\Delta\varepsilon = 2.849\,\mathrm{MeV}$ for $J^\pi = 1^+$ states. In $J^\pi = 3^+$ states, coupling to the continuum does not introduce any correction to the position of $1p_{1/2}$ s.p. state. Therefore, to obtain the energy and the wave function of $1p_{1/2}$ state we take the equivalent potential $U^{(eq)}(3^+)$ to $U^{(sc)}(3^+)$ for the $1p_{3/2}$.

In general, the surface region of average potential shows weak sensitivity to the self-consistent correction. Deviations from this general rule can be seen for weakly-bound many-body states having an important admixture of $l = 0$ and $l = 1$ neutron s.p. states, *i.e.*, for halo configurations in the neutron rich nuclei [32]. In this case, the self-consistent correction may change significantly the surface of the average potential [33]. In the above discussion we have considered effect of coupling between P and Q subspaces on the average s.p. potential for the proton orbits. To exclude the effect of Coulomb barrier, in Fig. 2 we show the initial potential $U(r)$, the self-consistent potential $U^{(sc)}(r)$, and the equivalent potential $U^{(eq)}(r)$ for neutron $1p_{3/2}$ s.p. orbit in ^{8}Li where, for the sake of argument, $1p_{3/2}$ neutron s.p. orbit in $U^{(sc)}(r)$ is at $-20\,\mathrm{keV}$. Parameters of the initial potential in this case are: $V_0 = -33.4\,\mathrm{MeV}$, $R_0 = 2.4\,\mathrm{fm}$, $a = 0.52\,\mathrm{fm}$ and $V_{SO} = -4\,\mathrm{MeV}$. Parameters of the residual interaction (3) are the same as used in Fig. 1. One may notice that the self-consistent correction to the average potential is now much stronger than in ^{8}B and, in particular, it changes strongly the surface of $U^{(sc)}(r)$, as expected for weakly-bound halo nuclei [32].

Fig. 3 shows the dependence of $U^{(sc)}(r)$ on the parameter $(1-\alpha)$ of the spin-exchange component of the two-body residual interaction (3). The self-consistent potentials for different values of $(1-\alpha)$ have been determined for the $1p_{3/2}$ s.p. proton orbital ($\varepsilon_{p_{3/2}} = -137\,\mathrm{keV}$) in $J^\pi = 2^+$. Parameters of corresponding initial potentials $U(r)$ are shown in Table I. We see that $U^{(sc)}(r)$ strongly depends on the the spin-exchange term of the residual force (3). The largest correction to the initial potential $U(r)$ is obtained for small values of $(1-\alpha)$, *i.e.*, when approaching the Wigner force limit. This dependence of $U^{(sc)}(r)$ on the spin-exchange component of the residual interaction has a sensible effect on the width of resonances, as we shall see below.

B. Spectrum of ^{8}B

In this section and in Sect. III.C, we shall present the detailed calculations of spectra for mirror nuclei : ^{8}B and ^{8}Li. The SMEC results depend on the following ingredients : (i) the nucleon - nucleon interaction in Q subspace, (ii) the residual coupling of Q and P subspaces, (iii) the self-consistent average s.p. potential which generates the radial formfactor for s.p. bound wave functions and s.p. resonances, and (iv) the cutoff radius for s.p. resonances. Fig. 4 compares SM energy spectrum for $T = 1$ states of ^{8}B (on the l.h.s.) calculated in the p - shell using the CK interaction [31] , with those obtained in the SMEC in different approximations. The experimental data are plotted on the r.h.s. of this figure. For the spin-exchange parameter in (3), we take $(1-\alpha) = 0.27$. Different sets of coupling matrix elements are taken into account. In the column denoted 'SMEC', we include coupling matrix elements between the $J^\pi = 3/2^-$ g.s. wave function of ^{7}Be and all considered states in ^{8}B. 'SMEC1' and 'SMEC1*' columns show the results when also coupling matrix elements between the $J^\pi = 1/2^-$ first excited state in ^{7}Be and states of ^{8}B are included. In 'SMEC1', this $J^\pi = 1/2^-$ state is at the energy ($E^* = 1.07\,\mathrm{MeV}$) predicted by SM, which differs from the experimental energy ($E^* = 0.429\,\mathrm{MeV}$) of this level. For that reason, in the column denoted 'SMEC1*', we show results of calculations where energy of $J^\pi = 1/2^-$ state is put at its experimental position, without changing neither the coupling matrix elements of residual force nor the effective interaction in Q subspace.

The iterative procedure to correct $U(r)$ and to include the diagonal part contribution of residual interaction has been described in the previous section. The self-consistently determined s.p. potential $U^{(sc)}(r)$ is then used to calculate the radial formfactors of coupling matrix elements and the s.p. wave functions. One and the same potential $U(r)$ is used for the calculation of self-consistent potentials for all many-body states in ^{8}B, and for both $1p_{3/2}$ and $1p_{1/2}$ proton s.p. states. These self-consistent potentials for $1p_{3/2}$ proton s.p. state in $J^\pi = 2^+$ and 1^+ states of ^{8}B can be seen in Fig. 1. For neutrons, there is no correction from the residual interaction, and the average s.p. potential is chosen such that

it yields $1p_{3/2}$ and $1p_{1/2}$ neutron orbits at $-13.02\,\mathrm{MeV}$ and $-11.16\,\mathrm{MeV}$ respectively. These values have been deduced from experimental Q-values and SM spectroscopic factors. The parameters of initial potential for neutrons are : $V_0 = -67.595\,\mathrm{MeV}$ (for $1p_{3/2}$ state) and $V_0 = -70.942\,\mathrm{MeV}$ (for $1p_{1/2}$ state). The remaining parameters are the same as for protons. The r.m.s. radius of neutron $1p_{3/2}$ and $1p_{1/2}$ orbitals is $< r^2 >^{1/2} \simeq 2.5\,\mathrm{fm}$. We have checked that this choice of potential parameters for neutrons is not crucial and, *e.g.*, shift of neutron s.p. energies by $\sim 2\,\mathrm{MeV}$ does not influence final results of SMEC for the spectroscopy of ^{8}B. Supplementary informations concerning results shown in Fig. 4 can be found in Table II.

The spectrum of ^{8}B is relatively insensitive to certain approximations in SMEC. Ground state energy relative to the proton emission threshold is reasonably well reproduced by the SMEC. Zero of the energy scale is fixed at the experimental position of $J^\pi = 1^+_1$ first excited state with respect to the proton emission threshold for all examples of SMEC calculations which are shown in Fig. 4. The position of g.s. with respect to the energy threshold for proton emission changes by about 100 keV due to the inclusion of coupling to the g.s. of ^{7}Be (compare columns denoted 'SM' and 'SMEC' in Fig. 4 and in Table II). The coupling to the excited ^{7}Be* nucleus is relatively unimportant (see columns denoted 'SMEC1' and 'SMEC1*' in Fig. 4 and in Table II). Calculated width of $J^\pi = 1^+_1$ depends weakly on chosen couplings (compare 'SMEC' with 'SMEC1' or 'SMEC1*' columns in Table II) and for the interaction with $(1 - \alpha) = 0.27$, one obtains approximately half of the experimental width. Width for $J^\pi = 1^+_1$ state depends sensitively on the proportion of direct and spin-exchange terms (see Fig. 5 and Table III) in the residual interaction, and the agreement with the experimental value improves when approaching the limit of Wigner force ($\alpha = 1$). (Other details can be read in Table III.) In this limit, the residual interaction V_{12} in (3) is compatible with SU(4) supermultiplet symmetry [34]. It is well known that this limit is badly broken in majority of heavier nuclei mainly due to the increasing importance of spin-orbit coupling. Significant deviations from SU(4) symmetry in nuclei heavier than ^{16}O have been found by comparing the realistic shell model wave function and the favoured SU(4) representation [35]. However, in p-shell nuclei, SU(4) is still a good approximation

[36,37]. The Gamow-Teller transitions have been studied using the SM calculations with CK interaction showing that the supermultiplet symmetry of SU(4) is well preserved [37]. Comparison of jj and LS couplings in terms of the ratio a/K of their respective energy scales suggested a gradual increase of a while going from light to heavy p-shell nuclei and, hence, the growing importance of jj coupling at the end of the p-shell [38]. On the other hand, realistic SM calculations have shown that the g.s. wave functions have very small admixture of SU(4) - breaking configuration , both at the beginning and at the end of p - shell [31,36,39]. Analysis of giant magnetic dipole resonance using the same realistic force have also shown that salient selection rules of SU(4) remain valid in p - shell nuclei [37]. For that reason, it is encouraging that SMEC calculations in ^{8}B for low-lying many body resonances and, in particular, the residual two-body interaction which couples Q and P subspaces, is consistent with these SM findings.

It is instructive to see the energy dependence of $J^\pi = 1_1^+$ lowest eigenvalue of the effective Hamiltonian (12) in ^{8}B (see Fig. 6) . The same interaction and potentials as in Fig. 4 are used. Results shown with the solid line include the coupling of $J^\pi = 1_1^+$ state to the channel wave function obtained by the coupling of $J^\pi = 3/2^-$ g.s. wave function of ^{7}Be with one proton scattering wave function. The dashed line shows results obtained by including couplings both to the g.s. and to the $J^\pi = 1/2^-$ first excited state of ^{7}Be at the energy given by the SM calculation. Finally, the dotted line shows the results when this first excited state is placed at the experimental position ($E^* = 0.429\,\mathrm{MeV}$). The real part of the eigenvalue depends on the total energy of the system. For the center of mass (c.m.) energies less than about 2 MeV, E_R is a decreasing function of energy and for higher energies it becomes an increasing function of energy. The minimum of $E_R(E)$ depends slightly on whether the coupling to the $J^\pi = 1/2^-$ first excited state of ^{7}Be is included. On the contrary, the imaginary part of the eigenvalue increases monotonously with energy from the threshold and saturates at higher energies. Different approximations concerning the couplings have an influence E_R and are practically insignificant for Γ_R.

SM energy of the first $J^\pi = 3_1^+$ level is too low as compared to the experimental value

(see Figs. 4 and 5). The coupling to the continuum cannot correct for this deficiency of SM. The width of 3_1^+ state differs by at least a factor 5 from the experimental data and here, again, the agreement between experiment and calculations improves when $\alpha \rightarrow 1$ (see Fig. 5 and Table III). There may be several reason for the observed discrepancy between SMEC calculations and the experimental data for this state. Firstly, as mentioned already, SM is not well describing energy of this state. (The CK interaction is somewhat less successful in describing spectra of light p-shell nuclei.) Secondly, the wave function of experimental 3_1^+ state is most probably overlapping with the cluster configuration [^{3}He$-^5$Li], which cannot be adequately described in p-space SM calculations. It is known in mirror nucleus ^{8}Li, that the 3_1^+ state is strongly influenced by the mirror cluster configuration [^{3}H $-$ ^{5}He] [40] . Moreover, energy of experimental 3_1^+ state lies above the threshold for three-particle decay: ^{8}B $\longrightarrow$ [^{3}He $-$ p $-$ ^{4}He]. This decay channel which surely contributes to the experimental width, cannot be taken into account in the one-particle approximation for scattering continuum. Also correlations which could be generated in Q subspace by the coupling to this three-particle decay channel are outside of considered model space. Thirdly, 3_1^+ state in ^{8}B cannot couple to the first excited state $1/2^-$ of ^{7}Be but could couple to higher excited, particle-unstable states such as $7/2^-$. These couplings cannot be treated fully consistently in SMEC, because the closeness condition (1) implies that states in $(N-1)$ - nucleus must be stable with respect to the particle emission.

C. Spectrum of ^{8}Li

Table IV compares SM energy spectrum with those obtained in the SMEC for $T = 1$ states of ^{8}Li. SM calculations in the p - shell (Q subspace) are done using CK interaction [31], like in the case of ^{8}B. Parameters of the residual interaction (3) are also the same as given in caption of Table II. Parameters of $U(r)$ are given in Table I. $U(r)$ is such that the neutron $1p_{3/2}$ s.p. state in $U^{(sc)}(r)$ is bound by 2.033 MeV in $J^\pi = 2_1^+$ state, similarly as the experimental g.s. of ^{8}Li. The $1p_{1/2}$ neutron state is then bound by 1.109 MeV. The r.m.s.

of $1p_{3/2}$ neutron s.p. orbit in $U^{(sc)}(r)$ is $< r^2 >^{1/2} \simeq 3.474\,\mathrm{fm}$. The same initial potential is used for calculation of self-consistent average potentials for all other many-body states in ^{8}Li and for both $1p_{3/2}$ and $1p_{1/2}$ neutron s.p. states.

Coupling to the continuum induces the renormalization of spin-orbit interaction. The energy splitting of $1p_{3/2}$ and $1p_{1/2}$ orbitals which equals : $\Delta\varepsilon = 2.302\,\mathrm{MeV}$ in $U(r)$, becomes $\Delta\varepsilon = 0.924\,\mathrm{MeV}$ in $U^{(sc)}(2^+)$, and $\Delta\varepsilon = 3.078\,\mathrm{MeV}$ in $U^{(sc)}(1^+)$. One should notice that these splittings are *different* from analogous splittings in ^{8}B (see the discussion in Sect 3.B). Hence, the coupling to the continuum breaks explicitly the mirror symmetry of spectra and wave functions of SM.

The dependence of self-consistent correction to the average potential on isospin of s.p. states, induces a salient dependence of neutron s.p. potential on proton s.p. potential. This dependence is very weak in the studied cases of ^{8}Li and ^{8}B. For protons, $U(r)$ is such that it yields $1p_{3/2}$ orbit at $-14.8\,\mathrm{MeV}$ and $1p_{1/2}$ orbit at $-13.9\,\mathrm{MeV}$. These values have been deduced, similarly as for ^{8}B, from the experimental Q-values and SM spectroscopic factors. The parameters of $U(r)$ are $V_0 = -73.066\,\mathrm{MeV}$ (for $1p_{3/2}$ state) and $V_0 = -78.058\,\mathrm{MeV}$ (for $1p_{1/2}$ state), and remaining parameters are the same as for neutrons.

In the column denoted 'SMEC' in Table IV, we include the coupling between $J^\pi = 3/2^-$ g.s. of ^{7}Li and all considered states of ^{8}Li. 'SMEC1' and 'SMEC1*' columns show the results when also the coupling between $J^\pi = 1/2^-$ first excited state in ^{7}Li and states of ^{8}Li are included. In 'SMEC1', this $J^\pi = 1/2^-$ state is at the SM energy : $E^* = 1.07\,\mathrm{MeV}$. This energy value differs from the experimental value : $E^* = 0.467\,\mathrm{MeV}$. For that reason, in 'SMEC1*' column we show results where the energy of $J^\pi = 1/2^-$ state is placed at its experimental position. The coupling matrix elements of the residual force (3) and the CK interaction in Q subspace remain unchanged in 'SMEC1' and 'SMEC1*' calculations.

The position of g.s. with respect to the energy threshold for neutron emission is weakly modified by the inclusion of coupling to the continuum. The energy shift in this case is smaller than the shift caused by the coupling to $J^\pi = 1/2^-$ excited state of ^{7}Li*. In general,

the coupling of ^{8}Li to ^{7}Li* plays more important role than the analogous coupling of ^{8}B to ^{7}Be* . Experimentally, 3_1^+ state in ^{8}Li lies above the neutron emission threshold and, for all different examples of SMEC results shown in Table IV, we have put this state at an experimental position with respect to the neutron emission threshold. Ground state energy with respect to the neutron emission threshold is not well reproduced by SMEC calculations. Energies of lowest three states : $J^\pi = 2_1^+, 1_1^+, 3_1^+$ in SM calculation, are too much compressed as compared to the data. On the other hand, the energy splitting between 3_1^+ state and the second excited state 1_2^+ is well reproduced. The width of 3_1^+ state does not depend on the chosen coupling matrix elements and is by factor ~ 10 too small as compared to the data. The width of $J^\pi = 1_2^+$ state depends also weakly on the coupling matrix elements (see columns denoted by 'SMEC1' and 'SMEC1*') and is comparable to the experimental decay width.

Fig. 7 compares SM energy spectrum for $T = 1$ states of ^{8}Li (on the l.h.s.) with those obtained in the SMEC for different parameters $(1 - \alpha)$ of the residual interaction (3). A satisfactory agreement with the data for the width of 1_2^+ state is obtained when approaching the limit of Wigner force ($\alpha = 1$). (More details can be found in Table V.). Also the width of 3_1^+ state improves largely and differs only by factor 3 from the data. We consider that this agreement is satisfactory in view of the obvious limitations : (i) SM is not well describing energy of this state, (ii) the wave function of the 3_1^+ state is strongly overlapping with the cluster configuration [^{3}H $-$ ^{5}He] which cannot be reliably described in p - shell calculations [40], and (iii) 3_1^+ state cannot couple to the first excited state $1/2^-$ of ^{7}Li but could couple to higher excited states, such as $7/2^-$, which are particle unstable and cannot be included in the SMEC model. One should notice that SMEC describes better 3_1^+ in ^{8}Li than in ^{8}B due to the fact that the three-particle decay channel in ^{8}Li is closed.

Contrary to the $J^\pi = 3_1^+$ state, the $J^\pi = 1_2^+$ state in ^{8}Li is well reproduced, in particular, when the parameter of spin-exchange component in the residual interaction (3) approaches the limit of the Wigner force. It is interesting to see the energy dependence of second eigenvalue 1_2^+ of the effective Hamiltonian (12). The results shown with the solid line in Fig.

8 include the coupling of $J^\pi = 1_2^+$ in ^{8}Li to the $J^\pi = 3/2^-$ g.s. of ^{7}Li. One neutron is in the continuum. The dashed line presents results obtained by including couplings both to the g.s. and to the $J^\pi = 1/2^-$ first excited state of ^{7}Li at the energy predicted by the SM. Finally, the dotted line shows the results when this first excited state is placed at the experimental position $E^* = 0.467\,\mathrm{MeV}$. Contrary to the the case of $J^\pi = 1_1^+$ lowest eigenvalue in ^{8}B, now also the imaginary part Γ_R of the eigenvalue depends on the chosen couplings.

IV. RADIATIVE CAPTURE PROCESSES INVOLVING ^{8}B AND ^{8}LI NUCLEI IN THE FINAL STATE

A. The ^{7}Be$(p,\gamma)^8$B reaction

The β^+ decay of ^{8}B , which is formed by the reaction ^{7}Be$(p,\gamma)^8$B at the c.m. energy of about 20 keV, is the main source of high energy solar neutrinos. In the absence of agreement between different experimental data for this reaction and in view of the disagreement between different measurements of solar neutrinos, the input of SSM [1] should be compared with the theoretical values. The cross-section for the reaction ^{7}Be$(p,\gamma)^8$B remains the main uncertainty in the input of the SSM.

In the SMEC, the initial wave Ψ_i for the system $[^7\mathrm{Be} + \mathrm{p}]_{J_i^\pi}$ is :

$$\Psi_i(r) = \sum_{l_a j_a} i^{l_a} \frac{\psi_{l_a j_a}^{J_i}(r)}{r} \Big[[Y^{l_a} \times \chi^s]^{j_a} \times \chi^{I_t} \Big]_{m_i}^{(J_i)} \tag{16}$$

and the final wave Φ_f for the system $[^8\mathrm{B}]_{J_f^\pi = 2^+}$ is:

$$\Psi_f(r) = \sum_{l_b j_b} A_{l_b s j_b}^{j_b I_b J_f} \frac{u_{l_b j_b}^{J_f}(r)}{r} \Big[[Y^{l_b} \times \chi^s]^{j_b} \times \chi^{I_t} \Big]_{m_f}^{(J_f)} . \tag{17}$$

I_t and s denote the spin of target nucleus and incoming proton, respectively. $A_{l_b s j_b}^{j_b I_b J_f}$ is the coefficient of fractional parentage and $u_{l_b j_b}^{J_f}$ is the s.p. wave in the many-particle state J_f . With the wave $\Psi_i(r)$ and $\Psi_f(r)$, we calculate the transition amplitudes:

$$\begin{aligned} T^{E\mathcal{L}} = C(E\mathcal{L}) i^{l_a} \hat{J}_f \hat{l}_b \hat{j}_b \hat{j}_a < \mathcal{L}\delta J_f m_f \mid J_i m_i >< l_b 0 \mathcal{L} 0 \mid l_a 0 > \\ \times W(j_b I_t \mathcal{L} J_i J_f j_a) W(l_b s \mathcal{L} j_a j_b l_a) I_{l_a j_a, l_b j_b}^{\mathcal{L}, J_i} \end{aligned} \tag{18}$$

for $E1$ and $E2$ and :

$$
\begin{aligned}
T^{M1} &= i^{l_a}\mu_N \hat{J}_f < 1\delta J_f m_f \mid J_i m_i > \\
&\times\Bigg\{ W(j_b I_t 1 J_i; J_f j_a)\hat{j}_a\hat{j}_b \\
&\left[\mu\left(\frac{Z_t}{m_t^2}+\frac{Z_a}{m_a^2}\right)\hat{l}_a\tilde{l}_a W(l_b s 1 j_a; j_b l_a) + (-1)^{jb-ja}2\mu_a \hat{s}\tilde{s}W(s l_b 1 j_a; j_b s)\right] \\
&+\mu_t(-1)^{J_f-J_i}\hat{I}_t\tilde{I}_t W(I_t j_b 1 J_i J_f I_t)\delta_{j_a j_b}\Bigg\}\delta_{l_a l_b} I^{0,J_i}_{l_a j_a, l_b j_b}
\end{aligned}
\tag{19}
$$

for $M1$ transitions, respectively. In the above formula, $\delta = m_i - m_f$, $\hat{a} \equiv \sqrt{2a+1}$, $\tilde{a} \equiv \sqrt{a(a+1)}$ and :

$$
I^{\mathcal{L},J_i}_{l_a j_a, l_b j_b} = \int u_{l_b j_b} r^{\mathcal{L}} \psi^{J_i}_{l_a j_a} dr \quad . \tag{20}
$$

The radiative capture cross section can then be expressed as:

$$
\sigma^{E1,M1} = \frac{16\pi}{9}\left(\frac{k_\gamma}{k_p}\right)^3\left(\frac{\mu}{\hbar c}\right)\left(\frac{e^2}{\hbar c}\right)\frac{1}{2s+1}\,\frac{1}{2I_t+1}\sum \mid T^{E1,M1} \mid^2 \tag{21}
$$

$$
\sigma^{E2} = \frac{4\pi}{75}\left(\frac{k_\gamma^5}{k_p^3}\right)\left(\frac{\mu}{\hbar c}\right)\left(\frac{e^2}{\hbar c}\right)\frac{1}{2s+1}\,\frac{1}{2I_t+1}\sum \mid T^{E2} \mid^2 \tag{22}
$$

where I_t and s denote the spin of target nucleus and the spin of incoming proton, respectively. μ stands for the reduced mass of the system.

Fig. 9 shows the calculated multipole contributions to the total capture cross section as a function of c.m. energy for different parameters of the residual interaction (3). In the upper part, the calculation is done for the same parameters of the residual interaction as used in the calculations of spectra shown in Fig. 4. In the lower part, the calculation is done for $(1-\alpha) = 0.05$, close to the Wigner force limit. The spectrum in this case was shown in Fig. 5. Parameters of the initial potential $U(r)$ in these two cases can be read from Table I. The proton threshold energy is adjusted to agree energies of calculated and experimental 1^+_1 state. The photon energy is then given by the difference of c.m. energy of $[\mathrm{p}\otimes{}^7\mathrm{Be}]_{J_i^+}$ system and the experimental energy of the 2^+_1 g.s. of ^{8}B. As can be realized from Fig. 9, the $E1$ and $E2$ contributions as well as the total cross-section are insensitive to the amount of spin-exchange in the residual force. On the contrary, the $M1$

contribution and particularly its resonant part, are strongly dependent on α. Ratio of $E2$ and $E1$ contributions at the position of 1^+_1 resonance is $8.15{\cdot}10^{-4}$ or $7.72{\cdot}10^{-4}$ depending on whether the spin-exchange parameter equals 0.27 (the upper part of Fig. 9) or 0.05 (the lower part of Fig. 9). The experimentally deduced value for this ratio $6.7^{+2.8}_{-1.9} \cdot 10^{-4}$ [42] is consistent with our finding but does not allow to distinguish between different spin-exchange parameters.

$E1$ component provides the main contribution to the total capture cross-section in the reaction $^7\mathrm{Be}(p,\gamma)^8\mathrm{B}$. This non-resonant contribution is a good measure of the spatial extension of 2^+_1 wave function, which in turn is determined by the extension of the proton $1p_{3/2}$ orbit. It is essential for the calculated cross-section that the $1p_{3/2}$ proton orbit in the self-consistent average potential is bound by 137 keV. Modification of this value by different choice of the depth parameter V_0 in $U(r)$, introduces the change in S^{E1} which can be much larger larger than the change due to uncertainties in the potential radius R_0 or its surface diffuseness a.

Fig. 10 shows the total S - factor as a function of the c.m. energy. The SMEC results have been obtained for $\alpha = 0.95$. Different multipole contributions to the total cross section for this parameter of the residual interaction (3) have been shown in the lower part of Fig. 9. Together with SMEC results for the S-factor, we show experimental data [6,7]. The low energy dependence of $S(E)$ can be fitted by [13]:

$$S(E) = S(0)\exp(\hat{\alpha}E + \hat{\beta}E^2) \quad . \tag{23}$$

In our case, the fit of $S(E)$ using (23) in the range of c.m. energies up to 100 keV yields $S(0) = 19.594$ eV·b, $\hat{\alpha} = -1.544\,\mathrm{MeV}^{-1}$, $\hat{\beta} = 6.468\,\mathrm{MeV}^{-2}$. As compared to the similar fit of S - factor calculated in the Generator Coordinate Method [13] , we find smaller $S(0)$ parameter and slightly bigger values for the parameters $\hat{\alpha}$ and $\hat{\beta}$. Recent experimental determination of S-factor [7] yields similar to ours low value for $S(0)$.

The ratio of $M1$ and $E1$ contributions for $\alpha = 0.95$ is: $\sigma^{M1}/\sigma^{E1} = 1.43{\cdot}10^{-3}$, $2.65{\cdot}10^{-3}$ and $1.90{\cdot}10^{-2}$ at 20, 100 and 500 keV, respectively. The resonant part of $M1$ transitions

yields $S^{M1} = 20.52$ eV·b at the 1_1^+ resonance energy. This $M1$-contribution to the astrophysical S-factor decreases fast and becomes $S^{M1} = 3.65{\cdot}10^{-1}$, $4.74{\cdot}10^{-2}$, $2.72{\cdot}10^{-2}$ eV·b at c.m. energies 500, 100, 20 keV, respectively. At the position of 1_1^+ resonance, the calculated S - factor ($S = 40.67$ eV·b) is smaller than measured by Filippone et al. [6] . This value , which is dominated by the $M1$-contribution, is proportional to the square of spectroscopic amplitude of p-states, which for the CK interaction is -0.352 and 0.567 for $p_{1/2}$ and $p_{3/2}$ respectively. Similar small values of spectroscopic amplitudes are obtained for Kumar [43] and PTBME [44] interactions (see also [15]).

The $E2$ contribution to the astrophysical factor was recently measured by Kikuchi et al. [45] who finds: $S^{E2} \simeq 0.0^{+0.8}_{-0}$ meV·b and $S^{E2} \simeq 0.0^{+3(+3.6)}_{-0}$ meV·b in the energy intervals from 1.25 to 1.5 MeV and from 1.5 to 1.75 MeV respectively. SMEC gives for this quantity $52 - 53$ meV·b and $53 - 71$ meV·b, in these two energy intervals respectively. Similar values for S^{E1} have been been found by Typel and Baur [46]. These values are by factor 10 larger than those determined by Kikuchi et al. [45] what remains a puzzle.

B. The ^{7}Li$(n,\gamma)^8$Li reaction

This mirror reaction to the above considered capture reaction: ^{7}Be$(p,\gamma)^8$B , together with a simultaneous description of energy spectra and particle decay widths of ^{8}B and ^{8}Li, provides another stringent test for SMEC calculations. The SM interaction and SM many-body wave functions (*e.g.* the spectroscopic amplitudes) are identical in both cases. The self-consistent one-body potentials which take into account residual coupling of Q and P subspaces and which determine the radial formfactors of s.p. wave functions used in the calculation of matrix elements of the residual interaction (3), are optimized in the same way in ^{8}B and in ^{8}Li. Finally, the parameters of direct and spin-exchange terms in the residual interaction (3) are also the same, so the modification of coupling matrix elements in ^{8}B and ^{8}Li is solely due to the different radial shape of s.p. wave functions in the corresponding self-consistent potentials for different J^π of many-body states. In the case of neutrons,

the integral in Eq. (20) is sensitive to the nuclear interior even in the low energy limit. From elastic scattering of neutrons the scattering lengths a_S, where S is the channel spin ($\vec{S} = \vec{s} + \vec{I}_t$, *c.f.* Eqs. (16) and (17)), are known to be [47]: $a_1 = 0.87 \pm 0.07\,\mathrm{fm}$ and $a_2 = -3.63 \pm 0.05\,\mathrm{fm}$. So for the s-wave in the initial channel we adopted procedure of Barker [48] of readjustment of appropriate s-wave scattering potentials in order to reproduce these experimental values of scattering lengths.

In Fig. 11 we show different multipole contributions to the total capture cross section as a function of c.m. energy for different parameters α of the residual interaction (3). The same parameters have been used for the mirror reaction: $^7\mathrm{Be}(p,\gamma)^8\mathrm{B}$ (see Fig. 9). In the lower part of Fig. 11, the calculation is done for the spin-exchange parameter equal $(1-\alpha) = 0.05$. The corresponding parameters of $U(r)$ can be found in Table I. Similarly as for ^{8}B, the neutron threshold energy is adjusted to agree energies of calculated and experimental 3_1^+ state. The photon energy in Fig. 11 is then given by the difference of c.m. energy of $[\mathrm{n} \otimes {}^7\mathrm{Li}]_{J_i^+}$ system and the experimental energy of the 2_1^+ g.s. of ^{8}Li . As can be seen in Fig. 11, the total cross-section and the $E1$ contribution in particular, are insensitive to the amount of spin-exchange in the residual force. The $E2$ contribution shows a weak sensitivity to the parameter α in the region of 1_2^+ resonance. The $M1$ contribution and in particular its resonant part, are strongly dependent on α. At the thermal neutron energies, $M1$ contributions for $(1-\alpha) = 0.23$ and 0.05 differ by approximately one order of magnitude.

Like for the mirror reaction $^7\mathrm{Be}(p,\gamma)^8\mathrm{B}$, the dominant contribution to the total capture cross-section in $^7\mathrm{Li}(n,\gamma)^8\mathrm{Li}$ reaction is the $E1$ component. Nevertheless, the $M1$ contribution in $^7\mathrm{Li}(n,\gamma)^8\mathrm{Li}$ is relatively more important, in particular near the 3_1^+ resonance. This is partially due to the smaller extension of $1p_{3/2}$ neutron s.p. orbit in the g.s. wave function of ^{8}Li ($1p_{3/2}$ neutron s.p. orbit is bound by 2.033 MeV in the g.s. of ^{8}Li) as compared to the extension of $1p_{3/2}$ proton s.p. orbit in the g.s. of ^{8}B. This strong binding of $1p_{3/2}$ neutron state in 2^+ states of ^{8}Li has also a direct consequence on calculated radiative capture cross section which becomes reduced, mainly its $E1$ component. One should also underline that in

low-energy reaction such as ^{7}Li$(n,\gamma)^8$Li , neutron penetrates interior region of the potential and, therefore, is more sensitive to the ratio of direct and spin-exchange terms in (3) and, indirectly, to the modifications of the interior of average potential by the coupling to the continuum (see Figs. 1 - 3).

Fig. 12 shows the total neutron capture cross-section as a function of the c.m. energy. The calculation is done for the same parameters of residual interaction (3) as used in Fig. 10 for the mirror reaction ^{7}Be$(p,\gamma)^8$B . Together with the SMEC results, we show the data of Nagai et al. [19] which measured the cross-section for the γ - decay to the g.s. of ^{8}Li. The calculation fits well the data at this energy. The low energy dependence of calculated total neutron capture cross section can be fitted by [49]:

$$\sigma(E) = \left(\frac{\mu_n}{2E}\right)^{1/2} \left(s_0 + s_1 E^{1/2} + s_2 E + \cdots\right) \quad , \tag{24}$$

where μ_n is the reduced mass of neutron and E is the c.m. energy in MeV. In the energy interval up to 100 keV SMEC results can be well fitted by three-parameter fit: $s_0 = 11.517$, $s_1 = -2.145$, $s_2 = -11.636$, when μ_n is expresed in a.m.u.

The ratio of $M1$ and $E1$ contribution is $\sigma^{M1}/\sigma^{E1} = 1.78{\cdot}10^{-3}$, $2.09{\cdot}10^{-2}$ and 1.09 at 20, 100 and 200 keV, respectively. The resonant part of $M1$ transitions which is overestimated in the calculation due to small calculated width for this state, yields the contribution of $\sigma^{M1} = 305.1$ μb at the 3^+_1 resonance energy. This contribution decreases fast and becomes $\sigma^{M1} = 13.8$, 0.426, $9.18{\cdot}10^{-2}$ μb at c.m. energies 200, 100, 20 keV, respectively.

V. CONCLUSIONS

In this work we have applied SMEC model for the microscopic description of spectra in ^{8}B and ^{8}Li, and low-energy radiative capture cross sections in mirror reactions: ^{7}Be$(p,\gamma)^8$B and ^{7}Li$(p,\gamma)^8$Li. The SMEC model, in which realistic SM solutions for (quasi-)bound states are coupled to the one-particle scattering continuum, is a development of CSM model [24,25] for the description of low excitation energy properties of weakly bound nuclei. For that reason, we use a realistic SM effective interaction in the Q subspace and introduce a residual

zero-range force with the spin-exchange included which couples Q and P subspaces. This deliberate choice of interactions implies that the finite-depth potential generating potentials in P and matrix elements of residual coupling (Q subspace), has to be determined self-consistently. The self-consistent iterative procedure yields new state-dependent average potentials and consistent with them new renormalized matrix elements of the coupling force. These renprmalized couplings and average potentials are then consistently used in the calculations of spectra and capture cross-sections, *i.e.*, both in Q and P subspaces. What should be taken for coupling between bound and scattering states is in principle not known and we have decided to use a schematic combination of Wigner and Bartlett forces. Varying the parameter of the spin-exchange component for a fixed intensity of the coupling, we came to the conclusion that most satisfactory description of experimental data is achieved for small contribution of the spin-exchange part, *i.e.*, approaching the limit of pure Wigner force. This finding is consistent with the results of SM which strongly suggest an approximate validity of $SU(4)$ symmetry in p-shell nuclei [31,36,37,39]. This proves also an intrinsic consistency in our model between the effective SM interaction, in our case the CK interaction, and the residual coupling between Q and P subspaces.

Simultaneous study of mirror system and reactions allows for a better understanding of the role that play different approximations and parameters in the model. The dependence of final results on radius, diffusivity and spin-orbit coupling parameters of the initial potential $U(r)$ is not terribly important and they can be taken from any reasonable systematics. Coupling to the excited configurations in the $(N-1)$ - daughter nucleus is somewhat more important in ^{8}Li than in ^{8}B. However, this coupling depends only on the wave function of daughter nucleus in the excited state and is totally insensitive to the exact energy position of these excited configurations. On the contrary, the depth of $U(r)$ has to be carefully adjusted so that the energy of s.p. orbit(s) in $U^{(sc)}(r)$ involved in the systems: $[n \bigotimes (N-1)]$ and $[p \bigotimes (N-1)]$, reflects the binding of g. s. in the nucleus N. This is very important for any quantitative analysis of the reaction cross-section. In the studied cases of ^{8}B and ^{8}Li , the correct identification of this s.p. orbit and hence the determination of an appropriate

depth parameter in $U(r)$ is simple because the SM spectroscopic factor in 2^+_1 g.s. is close to 1. Different binding of ^{8}B and ^{8}Li leads in SMEC model to different $U^{(sc)}(r)$ for corresponding many-body states in mirror nuclei. This in turn causes: (i) the breaking of initial mirror symmetry in SM spectra of these nuclei and (ii) the different effective spin-orbit splitting in self-consistent potentials for corresponding states in mirror nuclei.

SMEC model in the present form allows to describe microscopically the coupling to one-nucleon continuum. More complicated decay channels like, *e.g.*, those involving the α particle in the continuum or more than two particles in the asymptotic states are beyond the scope of this model. It is encouraging, however, that these possible shortcomings in the description of decay channels, as we have shown on the example of 3^+_1 resonances, are so unambiguously reflected in the calculated decay width for these states. In general, the decay width is particularly sensitive to the details of the SM wave functions involved and to the values of matrix elements of residual coupling so they provide a sensible test of the quality of SMEC wave functions and/or approximations involved.

The overall agreement between experimental data and SMEC calculations for studied nuclei is good proving the internal consistency of model assumptions and parameters. The astrophysical factor $S(0)$ for the reaction ^{7}Be$(p,\gamma)^8$B equals 19.424 eV·b which is close to the values reported by Filippone et al. [6] and Hammache et al. [7] but differs from many earlier experiments as well as from many theoretical analysis [12,14,15] . The low-energy dependence of $S(E)$ is slightly different from the one found by Descouvement and Baye [12] which is sometimes used in extrapolating the experimental results to the astrophysically relevant region. The calculated ratio of S^{E1} and S^{E2} contributions in the region of 1^+_1 resonance also agrees well with the data of Davids et al. [42]. Surprisingly, at higher energies ($E > 1.25\,\mathrm{MeV}$) the calculated $E2$ contribution differs by factor 10 from the reported value of Kikuchi et al. [45]. The results of Refs. [42] and [45] seem to us incompatible with each other.

The present studies have shown that SMEC results depend sensitively on very small number of parameters. Some of them, like the parametrization of the residual interaction

which couples states in Q and P subspaces, has been established in the present work. The others, related to the energy of s.p. states which determine the radial wave function of many-body states, are bound by the SM spectroscopic factors and experimental binding energy in studied nuclei. This gives us a confidence that SMEC can have large predictive power when applied to other p - shell nuclei and to other capture cross-sections in this region.

Acknowledgements

We wish to express our gratitude to S. Drożdż and I. Rotter for many stimulating discussions during the course of development of the SMEC model. We thank also P. Van Isacker for his interest in the present work. This work was partly supported by KBN Grant No. 2 P03 B 14010 and the Grant No. 76044 of the French - Polish Cooperation.

APPENDIX A: THE COUPLING POTENTIAL AND THE SOURCE TERM

To solve the coupled channel equations (4) in P subspace, one has to calculate the matrix elements $V_{\alpha\beta\gamma\delta}$ of the residual interaction (3) between states in Q and P subspaces. For the zero-range force including the spin exchanges, which was used in this work, we have:

$$\mathcal{V}^L_{\alpha\beta\gamma\delta}(r_1,r_2) = \mathcal{Z}^L_{\alpha\beta\gamma\delta}\frac{1}{r^2}\delta(r_1-r_2) \quad , \tag{A1}$$

where

$$\mathcal{Z}^L_{\alpha\beta\gamma\delta} = \frac{V^{(0)}_{12}}{4\pi}\left[(a-b)\mathcal{M}^{L1}_{\alpha\beta\gamma\delta} + (1-\delta_{\tau_\alpha\tau_\beta}\delta_{\tau_\gamma\tau_\delta})(a+b)\mathcal{M}^{L0}_{\alpha\beta\gamma\delta}\right] \tag{A2}$$

and angular two-body matrix element with isospin T can be expressed as [41] :

$$\begin{aligned}\mathcal{M}^{LT}_{\alpha\beta\gamma\delta} = & -\frac{1}{4}\left(1+(-1)^{l_\alpha+l_\beta-l_\gamma-l_\delta}\right)\frac{\hat{j}_\alpha\hat{j}_\beta\hat{j}_\gamma\hat{j}_\delta}{\hat{L}^2} \\ & \times\Big\{(-1)^{j_\beta+j_\delta+l_\beta+l_\delta}< j_\alpha-\frac{1}{2}\, j_\beta\frac{1}{2}|L0>< j_\gamma-\frac{1}{2}\, j_\delta\frac{1}{2}|L0>\left[1-(-1)^{L+T+l_\gamma+l_\delta}\right] \\ & -< j_\alpha\frac{1}{2}\, j_\beta\frac{1}{2}|L1>< j_\gamma\frac{1}{2}\, j_\delta\frac{1}{2}|L1>\left[1+(-1)^T\right]\Big\} \quad .\end{aligned} \tag{A3}$$

Any symbol containing the hat, like *e.g.* $\hat{j}$, means: $\hat{j}\equiv\sqrt{2j+1}$.

The channel-channel coupling in (4), (10) is taken into account through the matrix elements of the type:

$$v_{cc'}{}^{J} = -\sum_{L} \hat{L} \cdot \mathcal{V}^{L}_{\alpha\beta\gamma\delta} \langle (J_t j_\alpha)_J || \left[\left(a^\dagger_\alpha a^\dagger_\beta \right)^L \cdot (\tilde{a}_\gamma \tilde{a}_\delta)^L \right]^0 || (J'_t j_\gamma)_J \rangle \tag{A4}$$

The N-body matrix element in the above expression, is rewritten as :

$$\sum_{K} \hat{L}^2 \cdot \hat{K}^2 \cdot \left\{ \begin{array}{ccc} j_\alpha & j_\beta & L \\ j_\gamma & j_\delta & L \\ K & K & 0 \end{array} \right\} \cdot \langle (J_t j_\alpha)_J || \left[\left(a^\dagger_\alpha \tilde{a}_\gamma \right)^K \cdot \left(a^\dagger_\beta \tilde{a}_\delta \right)^K \right]^0 || (J'_t j_\gamma)_J \rangle \ , \tag{A5}$$

and the reduced matrix element in this latter formula is then expressed as :

$$\hat{J}^2 \cdot \left\{ \begin{array}{ccc} J_t & j_\alpha & J \\ J'_t & j_\gamma & J \\ K & K & 0 \end{array} \right\} \cdot \langle J_t || \left(a^\dagger_\beta \tilde{a}_\delta \right)^K || J'_t \rangle \cdot \langle j_\alpha || \left(a^\dagger_\alpha \tilde{a}_\gamma \right)^K || j_\gamma \rangle \ . \tag{A6}$$

The diagonal parts of this operator induce corrections which renormalize the s.p. average potential $U(r)$ (see Eq. (9)).

The source term in the inhomogeneous eqs. (10) takes into account the couplings of the type :

$$w^{(i)} = -\sum_{L} \hat{L} \cdot V^{L}_{\alpha\beta\gamma\delta} \langle (J_t j_\alpha)_J || \left[\left(a^\dagger_\alpha a^\dagger_\beta \right)^L \cdot (\tilde{a}_\gamma \tilde{a}_\delta)^L \right]^0 || \Phi^i_J \rangle \tag{A7}$$

$$= -\sum_{L} \hat{L} \cdot V^{L}_{\alpha\beta\gamma\delta} \langle (J_t j_\alpha)_J || \left[a^\dagger_\alpha \left(a^\dagger_\beta (\tilde{a}_\gamma \tilde{a}_\delta)^L \right)^{j_\alpha} \right]^0 || \Phi^i_J \rangle \tag{A8}$$

Again, the reduced matrix element in this expression is given as a coupled product of the two contributions:

$$\hat{J}^2 \cdot \left\{ \begin{array}{ccc} J_t & j_\alpha & J \\ J & 0 & J \\ j_\alpha & j_\alpha & 0 \end{array} \right\} \cdot \langle j_\alpha || a^\dagger_\alpha || 0 \rangle . \langle J_t || \left(a^\dagger_\beta (\tilde{a}_\gamma \tilde{a}_\delta)^L \right)^{j_\alpha} || \Phi^i_J \rangle \tag{A9}$$

This operator modifies both real and imaginary parts of eigenvalues of H^{eff}_{QQ} in Eq. (12), but does not change the s.p. average potential $U(r)$.

REFERENCES

[1] J.N. Bahcall and R.K. Ulrich, Rev. Mod. Phys. **60** (1988) 297.

[2] J.N. Bahcall, Nucl. Phys. **A 631** (1998) 29c.

[3] P.D. Parker, Phys. Rev. **150** (1966) 851.

[4] W. Kavanagh, Bull. Am. Phys. Soc. **14** (1969) 1209.

[5] F.J. Vaughn et al., Phys. Rev. **C 2** (1970) 1657.

[6] B.W. Filippone et al., Phys. Rev. Lett. **50** (1983) 452.

[7] F. Hammache et al., Phys. Rev. Lett. **80** (1998) 928.

[8] T. Motobayashi et al., Phys. Rev. Lett. **73** (1994) 2680;
N. Iwasa et al., J. Phys. Soc. Jpn. **65** (1996) 1256.

[9] T.A. Tombrello, Nucl. Phys. **71** (1965) 459.

[10] A. Aurdal, Nucl. Phys. **A146** (1970) 385.

[11] R.G.H. Robertson, Phys. Rev. **C7** (1973) 543.

[12] P. Descovement, and D. Baye, Nucl. Phys. **A487** (1988) 420.

[13] P. Descovement, and D. Baye, Nucl. Phys. **A567** (1994) 341.

[14] A. Csótó, K. Langanke, S.E. Koonin, and T.D. Shoppa, Phys. Rev. **C52** (1995) 1130.

[15] B.A. Brown, A. Csótó, and R. Sherr, Nucl. Phys. **A597** (1996) 66.

[16] F.M. Nunes, R. Crespo, and I.J. Thompson, Nucl. Phys. **A615** (1997) 69; ibid. **A627** (1997) 747;
F.M. Nunes, R. Crespo, and I.J. Thompson, nucl-th/9709070;
F. Nunes, R. Shyam, and I.J. Thompson, J. Phys. **G 24** (1998) 1575.

[17] W.L. Imhof, R.G. Johnson, F.J. Vaughn, and M. Walt, Phys. Rev. **114** (1959) 1037.

[18] M. Wiescher, R. Steininger, and F. Käppeler, Ap. J. **344** (1989) 464.

[19] Y. Nagai et al., Ap. J. **381** (1991) 444.

[20] J.H. Applegate, C.J. Hogan, and R.J. Scherrer, Phys. Rev. **D35** (1987) 1151;
J.H. Applegate, C.J. Hogan, and R.J. Scherrer, Ap. J. **329** (1988) 572.

[21] G.M. Fuller, G.J. Mathews, and C.R. Alcock, Phys. Rev. **D37** (1988) 1380.

[22] R.A. Malaney, and W.A. Fowler, Ap. J. **333** (1988) 14.

[23] N. Terasawa, and K. Sato, Prog. Theor. Phys. **81** (1989) 254;
N. Terasawa, and K. Sato, Ap. J. **362** (1990) L47.

[24] H.W. Bartz, I. Rotter, and J. Höhn, Nucl. Phys. **A 275** (1977) 111.

[25] H.W. Bartz, I. Rotter, and J. Höhn, Nucl. Phys. **A 307** (1977) 285.

[26] B. Fladt, K.W. Schmid and F. Grűmmer, Annals of Physics (N.Y.) **184** (1988) 254;
ibid. **184** (1988) 300.

[27] H.R. Kissener, I. Rotter, and N.G. Goncharova, Fortschr. Phys. **35** (1987) 277;
I. Rotter, Rep. Prog. Phys. **54** (1991) 635.

[28] C. Mahaux, and H. Weidenműller, *Shell-Model Approach to Nuclear Reactions* (Amsterdam: North-Holland) (1969).

[29] K. Bennaceur, F. Nowacki, J. Okołowicz, and M. Płoszajczak, J. Phys. **G24** (1998) 1631.

[30] V.V. Balashov, A.N. Boyarkina, and I. Rotter, Nucl. Phys. **59** (1964) 414.

[31] S. Cohen and D. Kurath, Nucl. Phys. **A 73** (1965) 1.

[32] P.G. Hansen and B. Jonson, Europhys.Lett. **4** (1987) 409;
K. Riisager, A.S. Jensen and P. Møller, Nucl. Phys. **A548** (1992) 393.

[33] K. Bennaceur, F. Nowacki, J. Okołowicz, and M. Płoszajczak, to be published.

[34] E. Wigner, Phys. Rev. **51** (1937) 106.

[35] J.B. French and J.C. Parikh, Phys. Lett. **B 35** (1971) 1;
P. Vogel and W.E. Ormand, Phys. Rev. **C 47** (1993) 623.

[36] P.T. Nang, Nucl. Phys. **A185** (1972) 413.

[37] N.C. Mukhopadhyay and F. Cannata, Phys. Lett. **B51** (1974) 225.

[38] D.H. Wilkinson, Proceedings of *The Robert A. Welsh Foundation Conferences on Chemical Research. I. The Structure of the Nucleus*, Houston, Texas, November 20-22, 1957, p.13.

[39] G. John and P. Kramer, Nucl. Phys. **A204** (1973) 203.

[40] H. Stöwe and W. Zahn, Nucl. Phys. **A289** (1977) 317.

[41] P.J. Brussaard and P.W.M. Glaudemans, *Shell-Model Applications in Nuclear Spectroscopy*, North-Holland Publishing Company (Amsterdam - New York - Oxford).

[42] B. Davids et al., nucl-ex/9803012.

[43] N. Kumar, Nucl. Phys. **A 235** (1974) 221.

[44] R.E. Julies et al., S. Afr. J. Phys. **15** (1992) 35.

[45] T. Kikuchi et al., Phys. Lett. **B 391** (1997) 261.

[46] S. Typel and G. Baur, Phys. Rev. **C50** (1994) 2104.

[47] J.E. Lynn, E.T. Jurney and S. Raman, Phys. Rev. **C44** (1991) 764.

[48] F.C. Barker, Aust. J. Phys. **33** (1980) 177.

[49] C. Rolfs and W.S. Rodney, *Cauldrons in the Cosmos*, (University of Chicago Press, 1988).

TABLES

TABLE I. Parameters of the initial potentials $U(r)$ (5) used in the calculations of self-consistent potentials $U^{(sc)}(r)$ for various parameters $(1-\alpha)$ of the spin-exchange term in the residual interaction (3). $U^{(sc)}(r)$ are constructed for various $T=1$, positive parity states in ^{8}B and ^{8}Li and for different single particle states: $1p_{3/2}$ and $1p_{1/2}$. For all cases the radius of the potential is $R_0 = 2.4\,\mathrm{fm}$, the diffuseness parameter is $a = 0.52\,\mathrm{fm}$, and the spin-orbit orbit parameter is $V_{SO} = -4\,\mathrm{MeV}$. The strength of the residual interaction (3) is $V_{12}^{(0)} = 650\,\mathrm{MeV{\cdot}fm^3}$, for all considered cases.

System	$\varepsilon_{p_{3/2}}$ [MeV]	$1-\alpha$	V_0 [MeV]
[p $\otimes$ ^{7}Be]	-0.137	0.45	-42.140
		0.27	-40.045
		0.05	-37.660
[n $\otimes$ ^{7}Li]	-2.033	0.45	-41.683
		0.27	-39.555
		0.05	-36.905

TABLE II. SM energies and SMEC energies and widths vs. experimental ones of ^{8}B nucleus. All units are in keV. The proton separation energy is adjusted in order to reproduce the energy of the lowest resonance state. Different labels denote as follows: 'SMEC' – only the ground state of ^{7}Be was taken into account in all couplings, 'SMEC1' – coupling to the first excited state in ^{7}Be was included with $E^* = 1.07\,\mathrm{MeV}$ (SM value), 'SMEC1*' – the same with excited ^{7}Be state at $E^* = 0.429\,\mathrm{MeV}$ (experimental value). Parameters of the residual interaction (3) are: $V_{12}^{(0)} = 650\,\mathrm{MeV{\cdot}fm^3}$, $\alpha = 0.73$. The cut-off radius is $R_{cut} = 5\,\mathrm{fm}$ except for the $p_{1/2}$ s.p. wave function in 1_1^+ many body states, which is in the continuum at about 300 keV above the threshold and for which larger cut-off was used $R_{cut} = 10\,\mathrm{fm}$. The numbers in parentheses are the widths of 3_1^+ state if this state would be placed at the experimental energy. For more details, see the Table I and the description in the text.

State	SM	SMEC		SMEC1		SMEC1*		experiment	
J^π	energy	energy	width	energy	width	energy	width	energy	width
2^+	−446	−356	—	−334	—	−329	—	−137.5±1.0	—
1^+	637	637	16.5	637	15.3	637	15.2	637±6	37±5
3^+	1246	1294	13.1	1237	12.5	1241	12.6	2183±30	350±40
			(25.2)		(25.8)		(25.8)		
1^+	2327	2153	240.2	2081	272.7	2080	309.0	*not known*	

TABLE III. The dependence of ^{8}B spectra on the relative strengths of direct and spin exchange parts of the residual interaction (3). Analogously to the entry 'SMEC' in Table II only ground state of ^{7}Be was taken into account. The entries in this table are labelled by the value of α parameter of the residual force. The numbers in parentheses as in Table II. For more details see Table I, the caption of Table II and the discussion in the text.

State	SM	$\alpha = 0.55$		$\alpha = 0.73$		$\alpha = 0.95$		experiment	
J^π	energy	energy	width	energy	width	energy	width	energy	width
2^+	−446	−418	—	−356	—	−320	—	−137.5±1.0	—
1^+	637	637	12.6	637	16.5	637	25.9	637±6	37±5
3^+	1246	1313	3.0	1294	13.1	1275	34.9	2183±30	350±40
			(5.6)		(25.2)		(67.4)		
1^+	2327	2299	115.9	2153	240.2	1899	398.9	*not known*	

TABLE IV. The same as in Table II but for ^{8}Li nucleus. The neutron separation energy is adjusted in order to reproduce the energy of the lowest resonance state. Different labels denote as follows: 'SMEC' – only the ground state of ^{7}Li was taken into account in all couplings, 'SMEC1' – coupling to the first excited state in ^{7}Li was included with $E^* = 1.07\,\mathrm{MeV}$ (SM value), 'SMEC1*' – the same with excited ^{7}Li state at $E^* = 0.467\,\mathrm{MeV}$ (experimental value). The numbers in parentheses are the widths of 1_2^+ state if this state would be placed at the experimental energy. For other informations see Table I, the the caption of Table II and the discussion in the text.

State	SM	SMEC		SMEC1		SMEC1*		experiment	
J^π	energy	energy	width	energy	width	energy	width	energy	width
2^+	−1471.1	−1437.09	—	−1346.4	—	−1345.6	—	−2033.8±0.3	—
1^+	−388.1	−418.9	—	−349.5	—	−351.5	—	−1053.0±0.1	—
3^+	221.2	221.2	3.4	221.2	3.5	221.2	3.5	221.2±3.0	33±6
1^+	1301.6	1065.6	357.9	1050.0	383.1	1036.7	464.2	1176	≈ 1000
			(378.1)		(422.9)		(506.8)		

TABLE V. The dependence of ^{8}Li spectroscopy on the relative strengths of direct and spin exchange parts of the residual interaction is presented. Analogously to the entry 'SMEC' in Table IV, only g.s. of the ^{7}Li was taken into account. The entries in this table are labelled by the value of α parameter of the residual force. The numbers in parentheses as in Table IV. For other informations see Table I, the the caption of Table IV and the discussion in the text.

State	SM	$\alpha = 0.55$		$\alpha = 0.73$		$\alpha = 0.95$		experiment	
J^π	energy	energy	width	energy	width	energy	width	energy	width
2^+	−1471.1	−1514.7	—	−1437.9	—	−1330.3	—	−2033.8±0.3	—
1^+	−388.1	−441.7	—	−418.9	—	−394.4	—	−1053.0±0.1	—
3^+	221.2	221.2	0.8	221.2	3.4	221.2	9.4	221.2±3.0	33±6
1^+	1301.6	1199.2	171.8	1065.6	357.9	790.0	561.1	1176	≈ 1000
			(170.1)		(378.1)		(735.3)		

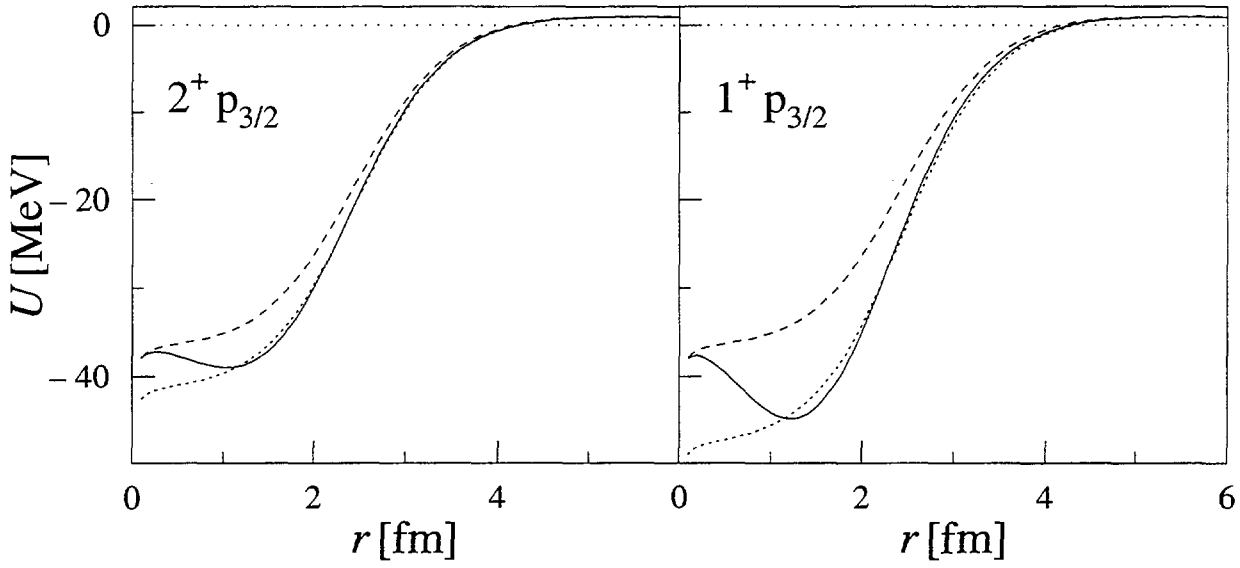

FIG. 1. Finite-depth average s.p. potentials used to generate the radial s.p. wave functions for bound states and resonances.

(i) Plot on the l.h.s. shows the initial potential $U(r)$ (5) (the dashed line), the self-consistent potential $U^{(sc)}(r)$ (the solid line), *i.e.*, $U(r)$ which is corrected by the coupling to the continuum of scattering states, and the equivalent average potential $U^{(eq)}(r)$ (the dotted line) of the Saxon-Woods type which yields the proton $1p_{3/2}$ orbit at the same energy as in the self-consistent potential. The residual interaction (3) parameters are: $V_{12}^{(0)} = 650\,\mathrm{MeV{\cdot}fm^3}$, $\alpha = 0.73$. $U(r)$ is chosen in such a way that $U^{(sc)}(r)$ yields the $1p_{3/2}$ s.p. state at the energy $-137\,\mathrm{keV}$, corresponding to the binding energy of the 2_1^+ g.s. in ^{8}B. The correction to the average potential from the residual interaction (3) is calculated for the $1p_{3/2}$ s.p. orbit in 2^+ states of ^{8}B. For more details, see Table I and the description in the text.

(ii) Plot on the r.h.s. shows the same as on l.h.s. but for the 1^+ states of ^{8}B. The initial potentials on the r.h.s. and l.h.s. are identical and $U^{(eq)}(r)$ is reproducing the position of the $1p_{3/2}$ s.p. orbit of $U^{(sc)}(r)$ for 1^+ states in ^{8}B.

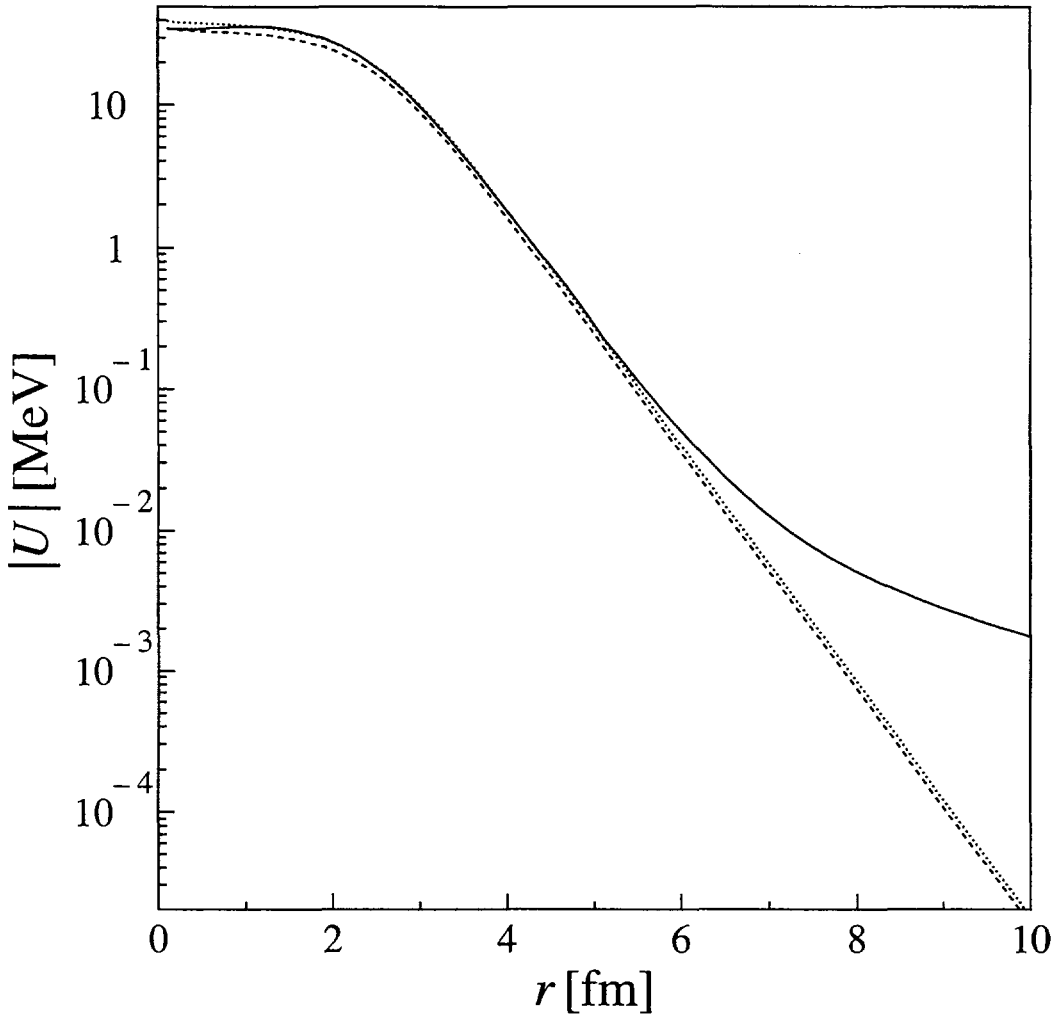

FIG. 2. The initial potential $U(r)$ of Saxon-Woods type (see (5)) (the dashed line), the self-consistent potential $U^{(sc)}(r)$ (the solid line) and the equivalent Saxon-Woods average potential $U^{(eq)}(r)$ (the dotted line) which yields the neutron $1p_{3/2}$ orbit at the same energy as found in $U^{(sc)}(r)$. The curves show the absolute value of corresponding potentials in the logarithmic scale so the characteristic tail for large r can be well seen. $U(r)$ is chosen in such a way that $U^{(sc)}(r)$ for neutrons obtained from it by including the diagonal correction term from the residual interaction (3) yields the $1p_{3/2}$ neutron s.p. state in $J^\pi = 2^+$ states of ^{8}Li at the energy $-20\,$keV. For more details, see Table I and the description in the text.

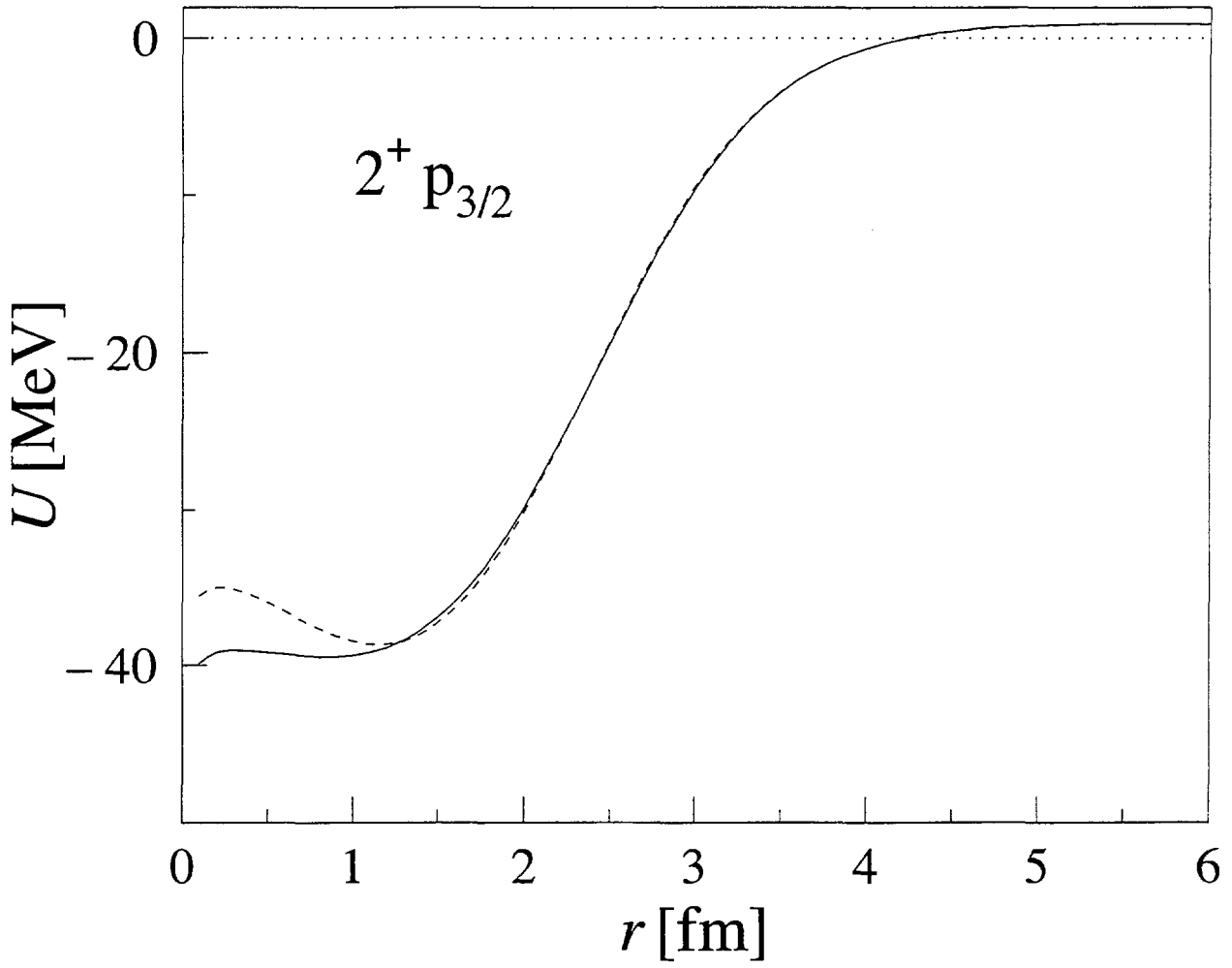

FIG. 3. The self-consistent average potential $U^{(sc)}(r)$ which is obtained by including the coupling of states in Q and P subspaces with the residual interaction (3), is plotted for two parameters of the residual force $\alpha = 0.55$ (the solid line) and $\alpha = 0.95$ (the dashed line). The calculations have been done for the s.p. orbit $1p_{3/2}$ and in $J^\pi = 2^+$ states of ^{8}B. The initial potential in each case has been chosen in such a way that the corresponding self-consistent potential yields the $1p_{3/2}$ s.p. orbit at the same energy of -137 keV. For more details, see Table I and the description in the text.

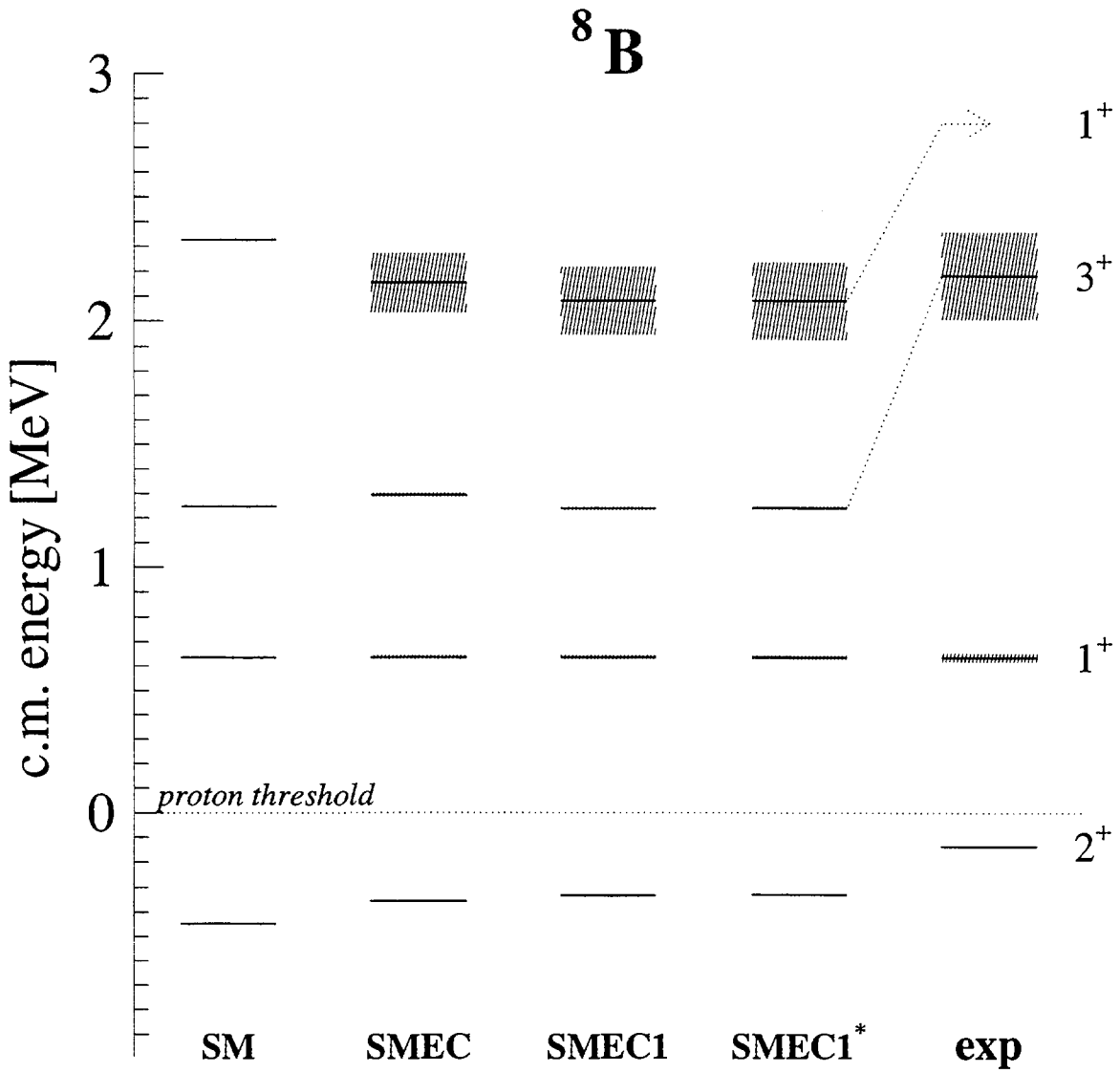

FIG. 4. SM with CK interaction and SMEC in different approximations labelled 'SMEC', SMEC1' and 'SMEC1*' vs. experimental $T = 1$ states of ^{8}B nucleus. The proton threshold energy is adjusted to reproduce position of the 1^+_1 first excited state. The shaded regions represent the width of resonance states. For the details of the calculation, see the description in the text and in the caption of Table I.

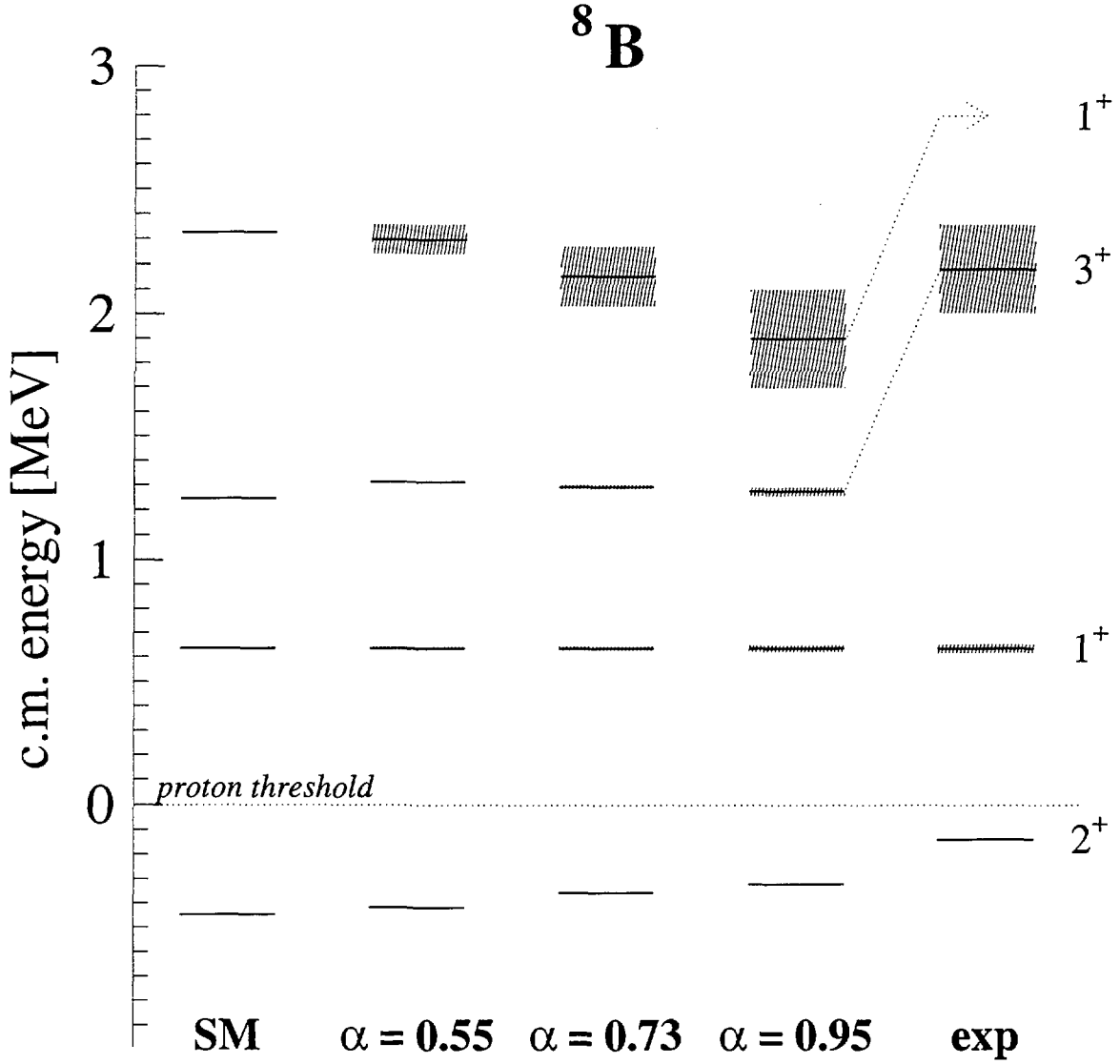

FIG. 5. Results of SMEC calculations for different parameters of spin-exchange part of the residual interaction in ^{8}B.

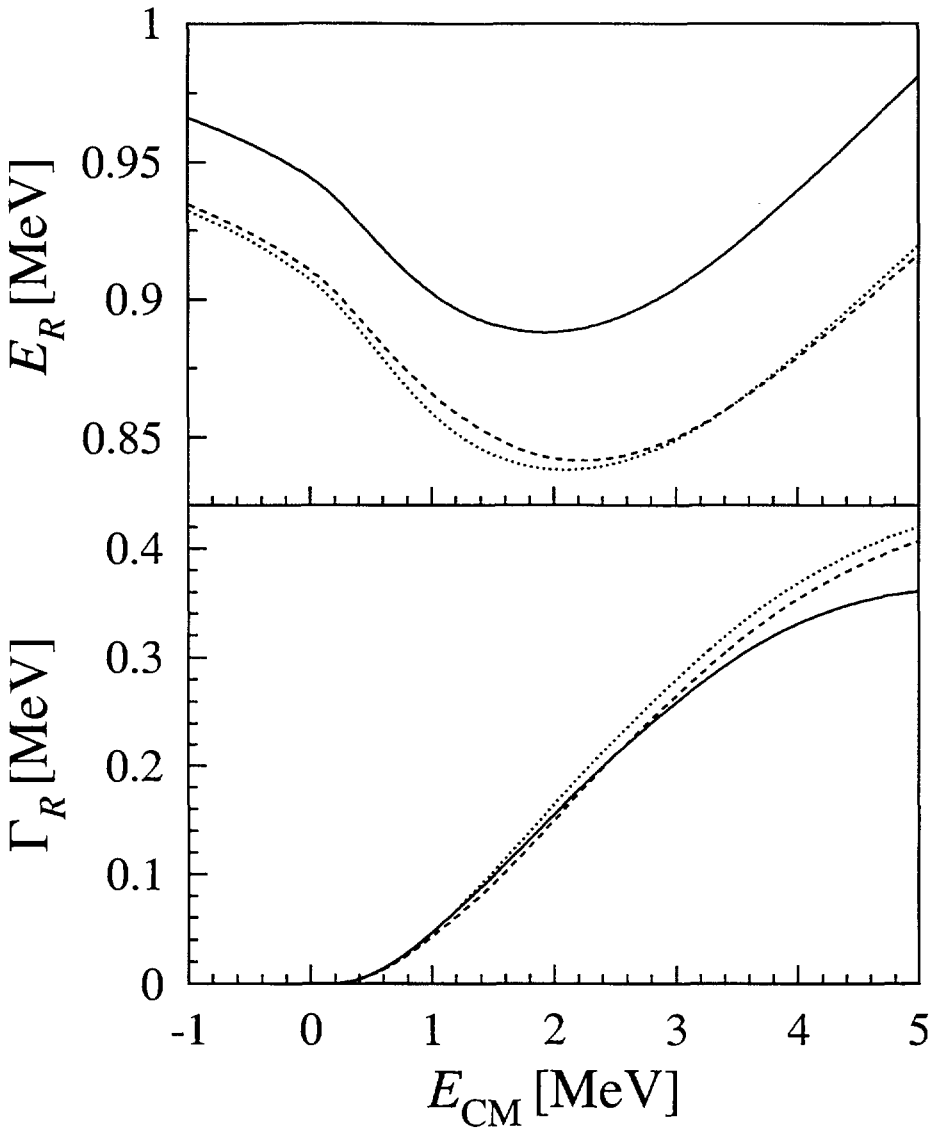

FIG. 6. Energy dependence of the eigenvalue (both real E_R and imaginary Γ_R parts) of the effective Hamiltonian (12) for the 1_1^+ state in ^{8}B. The solid line corresponds to the coupling to the g.s. of ^{7}Be only. The dashed line corresponds to the inclusion of coupling to the first excited state in ^{7}Be at the energy predicted by SM with CK interaction [31]. The dotted line corresponds to the inclusion of coupling to the first excited state in ^{7}Be which is placed at the experimental energy. For more details, see the description in the text.

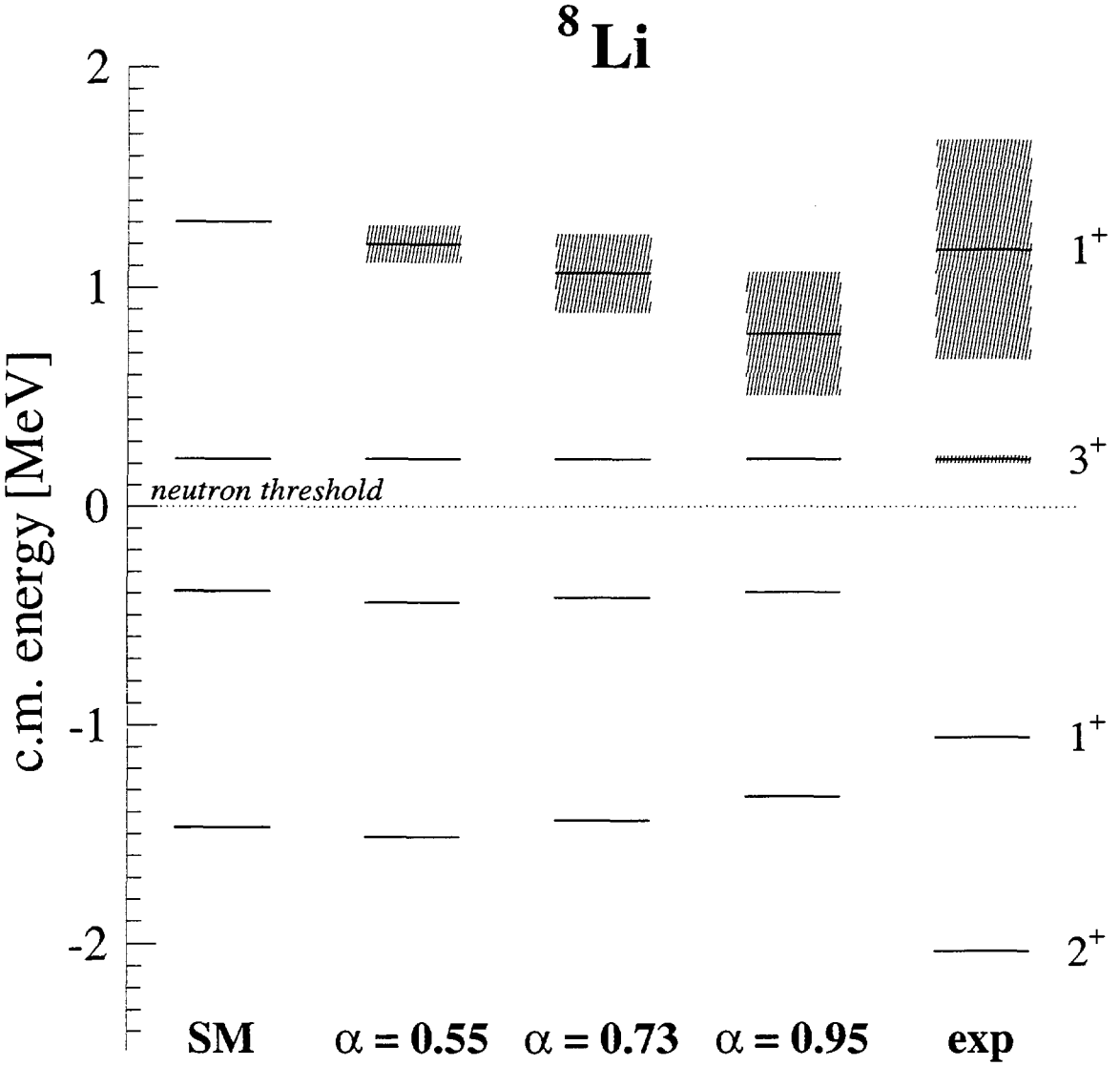

FIG. 7. Results of SMEC calculations for different parameters of spin-exchange part of the residual interaction in ^{8}Li.

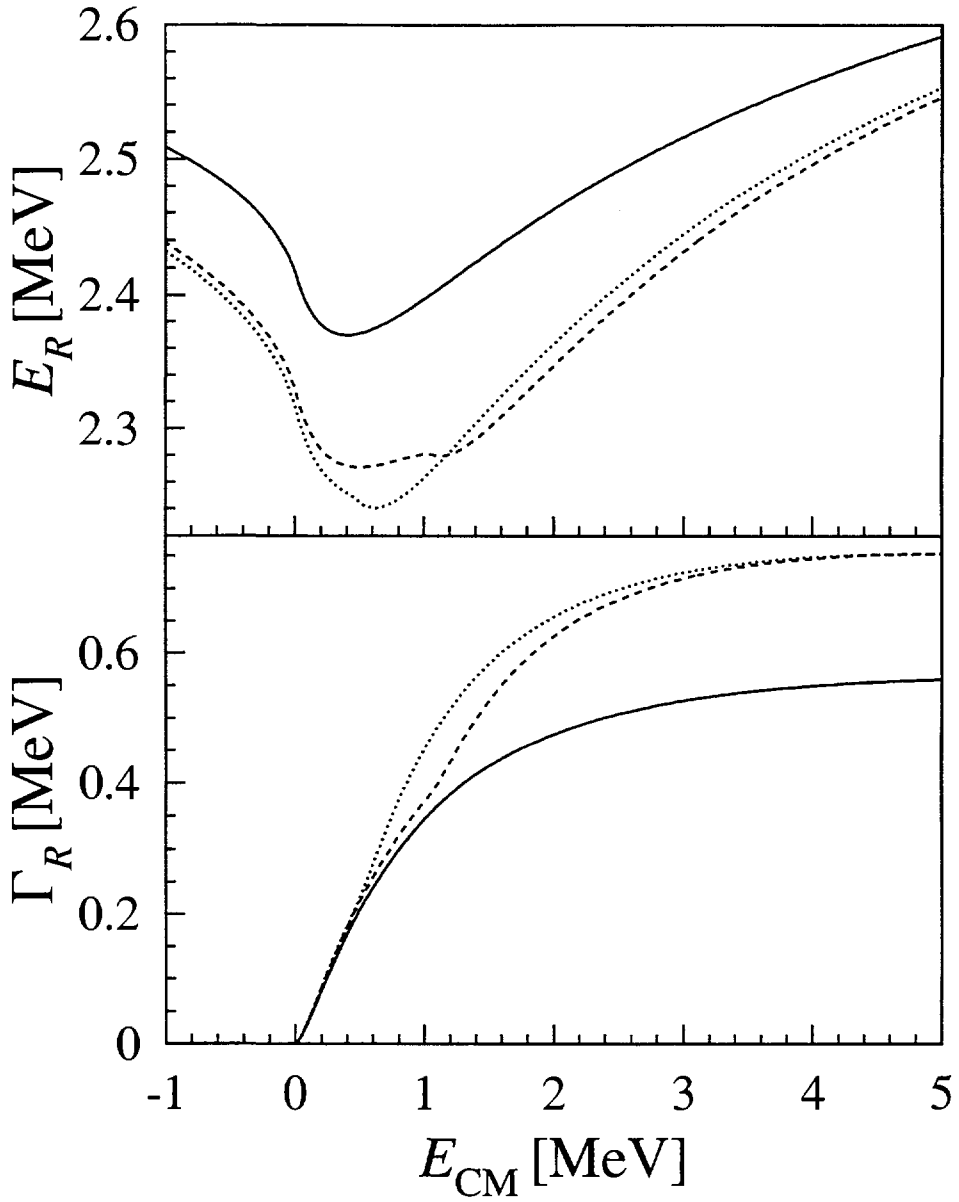

FIG. 8. The same as in Fig. 6 but for the 1_2^+ state in ^{8}Li. For more details, see the caption of Fig. 6 and the description in the text.

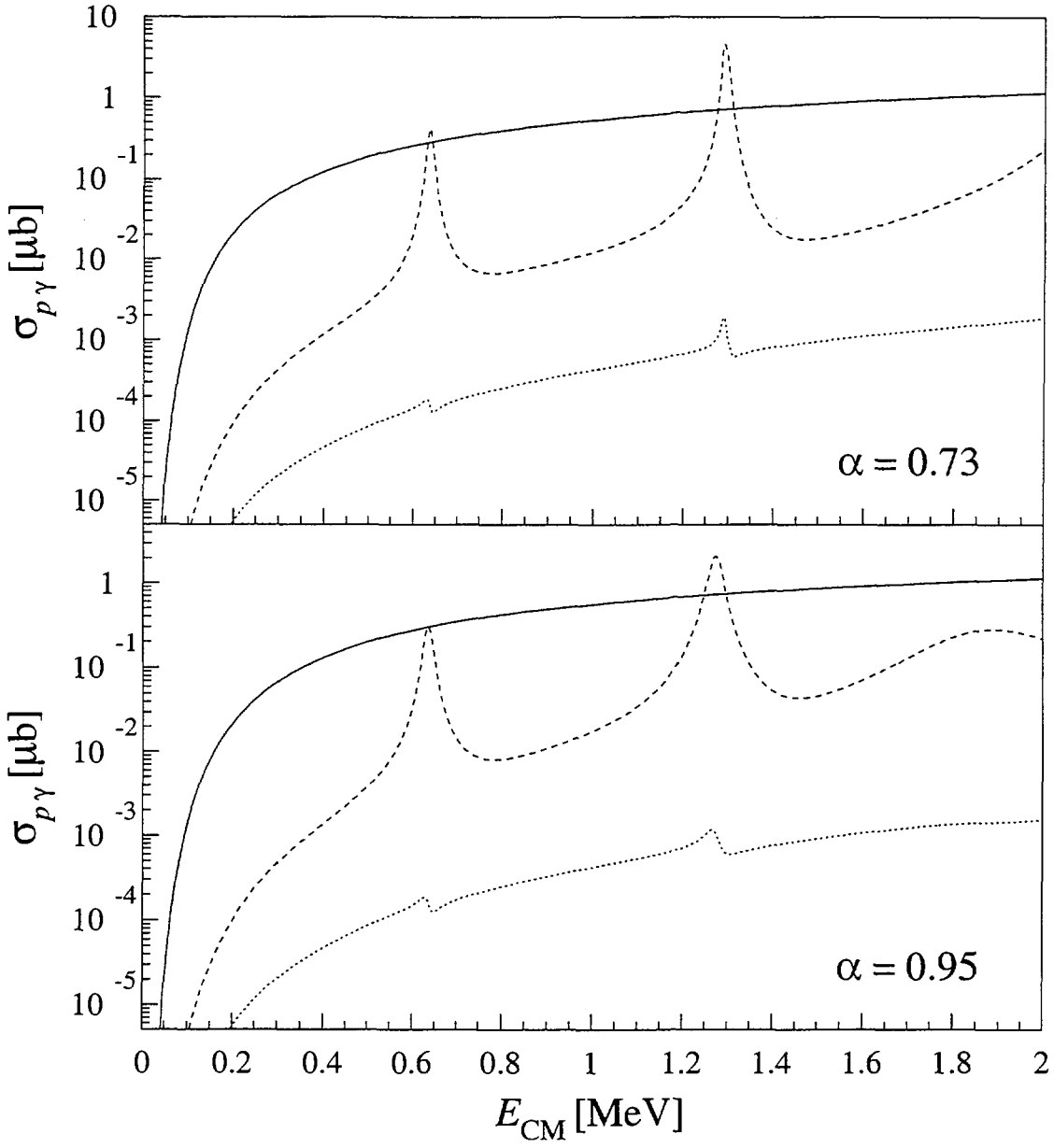

FIG. 9. Multipole contributions to the total capture cross section of ^{7}Be$(p,\gamma)^8$B as a function of the center of mass energy. The SMEC calculations have been done for different values of the spin-exchange parameter $(1-\alpha) = 0.27$ (the upper part of the figure) and $(1-\alpha) = 0.05$. For other details, see Table I and the discussion in the text.

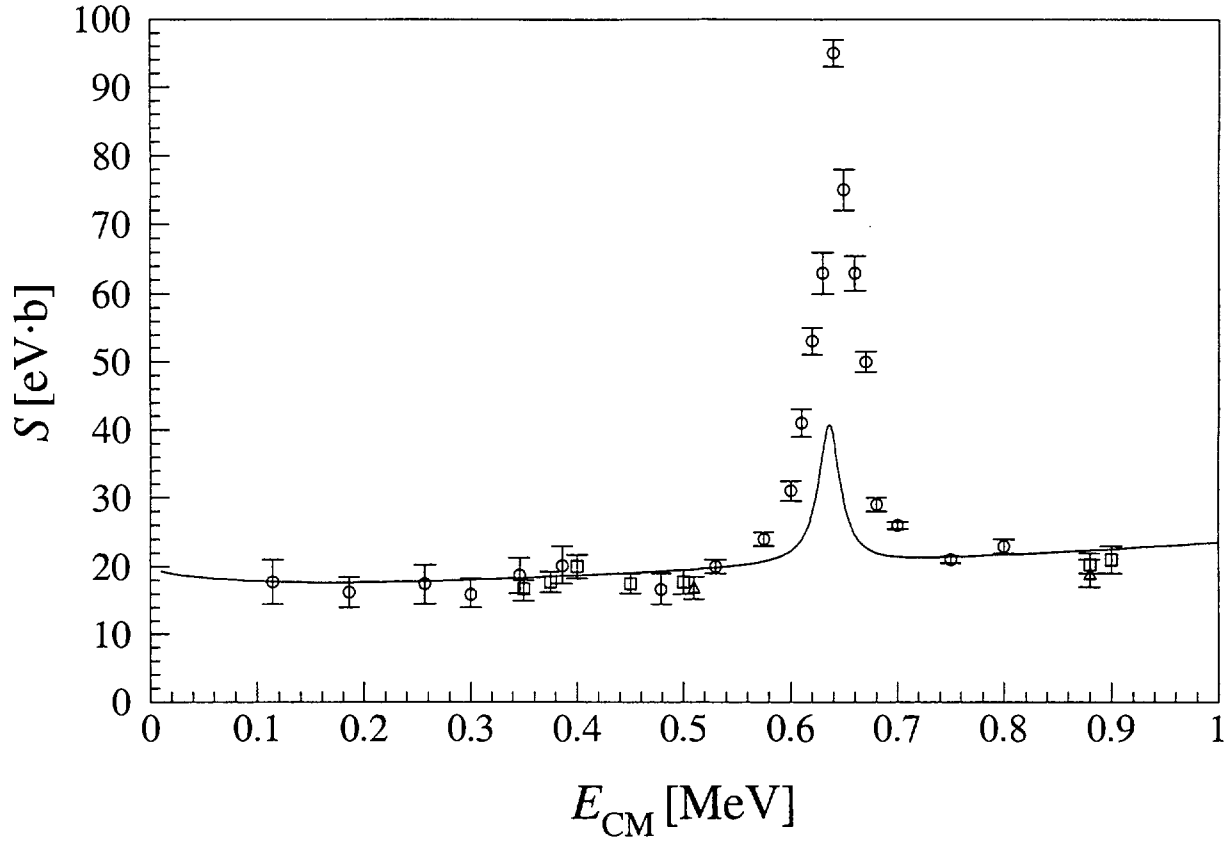

FIG. 10. The astrophysical S-factor for the reaction $^7\mathrm{Be}(p,\gamma)^8\mathrm{B}$ is plotted as a function of the center of mass energy. The SMEC calculations have been done for the residual interaction (3) the spin-exchange parameter $(1-\alpha) = 0.05$. The experimental points have been taken from Filippone et al. [6] and Hammache et al. [7].

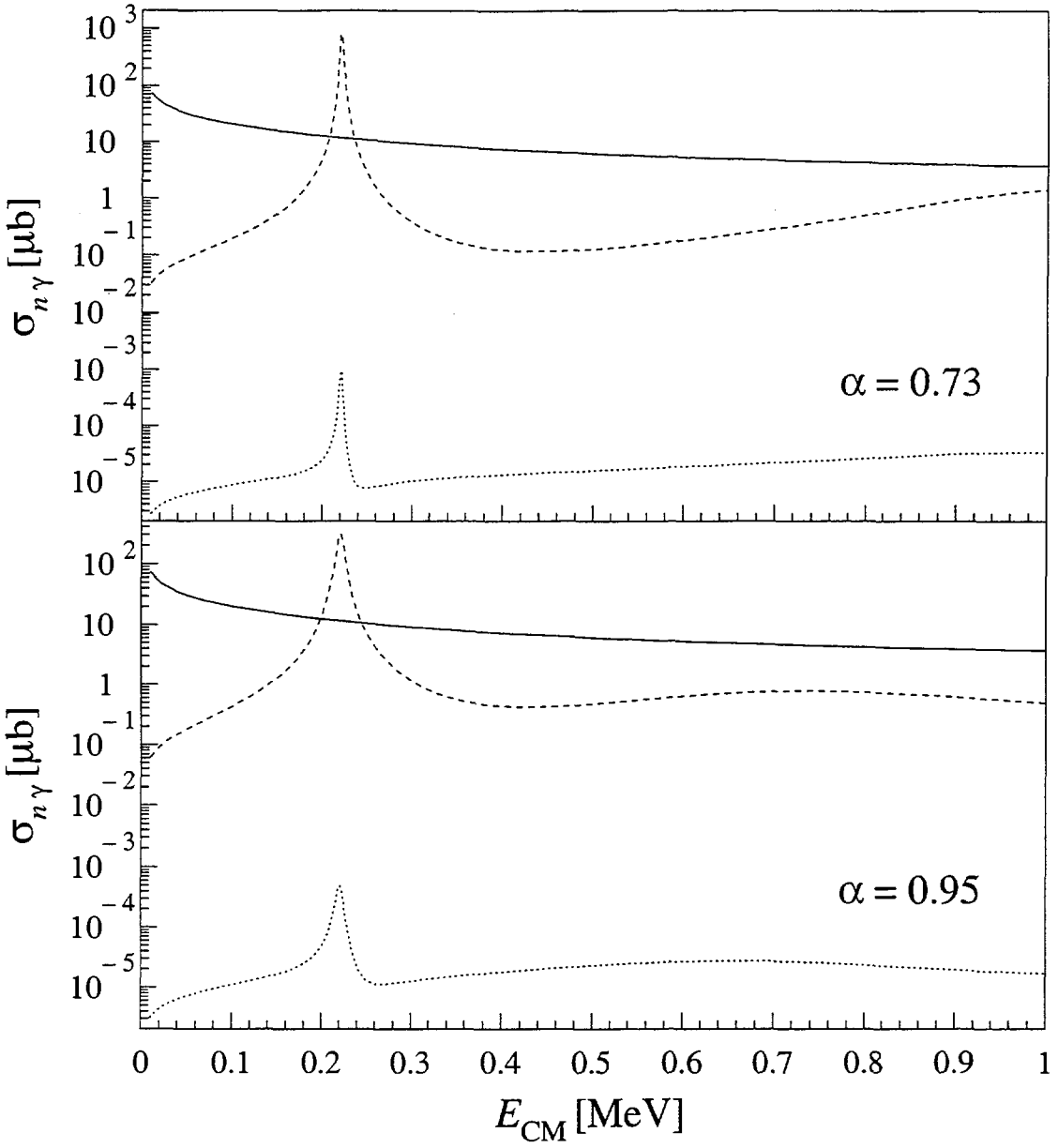

FIG. 11. Multipole contributions to the capture cross section to the g.s. ($J^\pi = 2_1^+$) of ^{8}Li in the reaction $^7\mathrm{Li}(n,\gamma)^8\mathrm{Li}$ are plotted as a function of c.m. energy. The SMEC calculations have been done with the spin-exchange parameter $(1-\alpha) = 0.27$ (the upper part of the figure) and $(1-\alpha) = 0.05$. For other details see the discussion in the text.

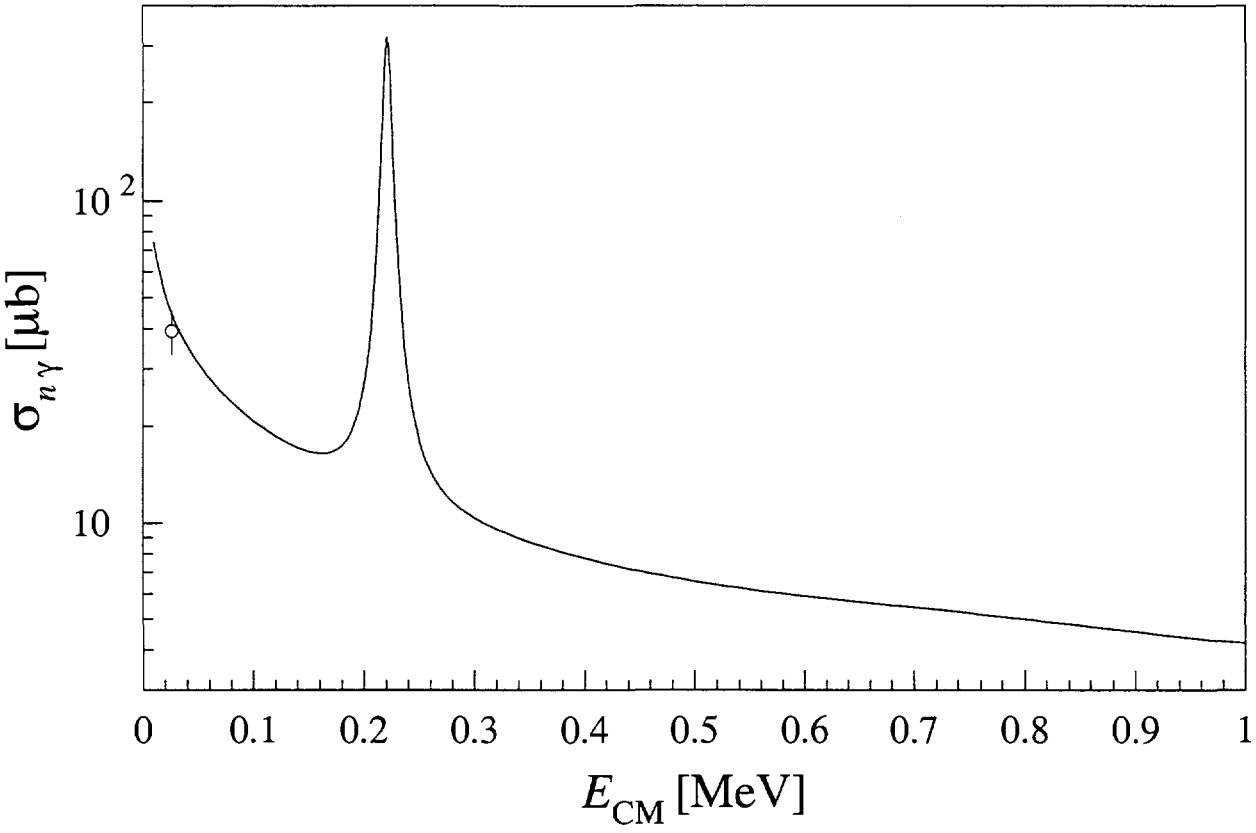

FIG. 12. The cross-section for the reaction $^7\mathrm{Li}(n,\gamma)^8\mathrm{Li}$ is plotted as a function of c.m. energy. The SMEC calculations have been done for the spin-exchange parameter $(1-\alpha) = 0.05$. The experimental point is taken from Nagai et al. [19].